A STUDY OF YIELDING AND PLASTIC FLOW IN POLYCRYSTALLINE NIOBIUM USING ACOUSTIC EMISSION AND ETCH PITS TECHNIQUES

BY

BRENT R. JUNKIN

A THESIS SUBMITTED TO THE FACULTY OF GRADUATE STUDIES
IN PARTIAL FULFILLMENT OF THE REQUIREMENTS FOR
THE DEGREE OF MASTER OF SCIENCE OF MECHANICAL ENGINEERING

DEPARTMENT OF MECHANICAL ENIGINEERING
UNIVERSITY OF MANTIOBA

WINNIPEG, MANITOBA

JULY, 1976

"A STUDY OF YIELDING AND PLASTIC FLOW IN POLYCRYSTALLINE NIOBIUM USING ACOUSTIC EMISSION AND ETCH PITS TECHNIQUES"

by

BRENT R. JUNKIN

A dissertation submitted to the Faculty of Graduate Studies of the University of Manitoba in partial fulfillment of the requirements of the degree of

MASTER OF SCIENCE

TABLE OF CONTENTS

ABSTRACT

The yielding and flow behaviour of polycrystalline 99.9% pure Nb has been investigated. Emphasis has been placed on the dependence of deformation phenomena on grain size. Etch pitting, acoustic emission and microstrain measurement techniques have been used to investigate the deformation behaviour.

Dislocations in Nb are initially produced at a stress level significantly lower than that of the microyield stress (6×10^{-6} strain) and that these dislocations are nucleated by two different types of sources. Grain boundary ledge sources result in slip lines in coarse grained material, and sources within the grains, probably grown in dislocations, result in a homogeneous distribution of new dislocations in both coarse and fine grained material.

The stress required for slip line initiation increases with decreasing grain size. This is attributed to an increase in ledge size with grain size, which results in higher stress concentrations in coarse grain sample grain boundaries. Therefore, a lower applied stress is necessary to activate these sources in coarse grained material. Slip bands form as a result of cross slip.

The microyield stress (at 6×10^{-6} plastic strain) shows a Hall Petch relationship in terms of grain size. The dislocation density is higher in finer grain sizes due to a shorter slip distance. Grain boundary source activation is more difficult in fine grain sizes because of a smaller ledge size, therefore, higher stresses are required to obtain the

required dislocation density. Acoustic emission results are in agreement with this hypothesis since the total emissions up to the upper yield point increase with decreasing grain size indicating that source activation follows the same trend.

Lüders band propagation is mainly the result of cross slip and easy slip between grains. This is reflected in the acoustic emission results by a substantial decrease in amplitude and number of emissions after the upper yield point is reached. The end result is that little or no grain size dependence of σ_{ly} is observed.

The flow stress and subsequently the dislocation process in the work hardening region are not grain size dependent. Smaller grain size samples have higher rates of acoustic emission. This is ascribed to the development of finer substructures and a smaller free flight distance for dislocations in fine grained samples.

ACKNOWLEDGEMENT

I wish to express my sincere thanks to Dr. K. Tangri for his patient guidance throughout the course of this work.

The advice of Mr. D. Mardis and the encouragement of my parents is greatfully acknowledged.

LIST OF FIGURES

LIST OF TABLES

1.0 Introduction

The mechanical behaviours of metals with the body centered cubic structure has been extensively studied in the past. By virtue of the fact that Fe-Si contains a limited number of glide systems and is easily etch pitted, it has been considered a model for plasticity studies in b.c.c. materials. Much information on the nature of grain boundaries and their effects on the grain size dependence of the yielding behaviour of metals has been due to investigations of Fe-Si. However, another b.c.c. metal, Niobium, shows little or no grain size dependence when typical heat treatments are used to give a variety of grain sizes, and subsequently the theories of yielding developed from Fe-Si studies do not apply. Only modest progress has been made in explaining grain size independence of the flow stress in Nb. Studies have shown that mobile dislocations are initially produced from regions near the grain boundaries, however, no satisfactory explanation of the grain size independnece of the flow stress has been forthcoming which doesn't involve impurity variations with grain size.

The purpose of the present work on polycrystalline Nb is to document and explain the observed phenomena during straining in the microyield and macroyield regions of the stress strain curve.

Etch pit and acoustic emission techniques have been used to investigate initial dislocation activity and to study dislocation activity as strain increases in the specimens. The observations made of initial dislocation activity, first slip line formation, the microyield stress

2.0 Review of Prior Work

The main concern of this section is to review previous research on the deformation of Niobium (Nb) relevant to the current study. Areas of special consideration include: the annealed structure, the deformation mechanisms in both micro- and macro-yield regions, the grain size effect on the flow stress, and the effect of impurity content on the deformation behaviour.

Some pertinent details on the deformation mechanisms of another b.c.c. metal, Iron-silicon, are included in this review for purposes of comparison. It must be emphasized that differences exist between the deformation mechanisms of Fe-Si and Nb.

Fe-Si has a low stacking fault energy, and slip is restricted to the (110) slip system.

The stacking fault energy is high in Nb and the (101), (123) and (112) slip planes are all active.

Where appropriate, results of experiments on Iron-silicon have been included in this review to enhance understanding of yielding phenomena.

2.1 Annealed Structure

Due to the fact that Nb has high affinity for Oxygen, Nitrogen, Hydrogen and Carbon, annealing treatments must be done under vacuum or in inert atmosphere. Temperatures used have ranged from approximately $960^{o}C$ to just below the melting point ($2400^{o}C$), resulting in grain diameters of .008 mm to single crystals. Grains usually appear well formed, with relatively equiaxed grain boundary junctions.

Evans (1) has reported that the etch-pit density due to grown-in dislocations, i.e., those in the annealed structure was found to decrease markedly with an increase in annealing temperature. A cursory examination indicated that in samples which were annealed from 1400^{o}C to 1600^{o}C, resulting in .25 to 950 grains/mm^2, there was at least a ten-fold decrease in the number of etch pits observed. In the coarse-grained material, concentrations of etch-pits were often found at grain corners. Etch pits in grains adjacent to one another often exhibited the same shape and orientation, suggesting that grains are also closely orientated.

Vardiman and Achter (2) investigated dislocation structures in Nb single crystals by using optical microscopy of doped surface layers and etch pitting techniques. It was found that triangular pits require the presence of carbon to be electro-etched and are confined to orientations in the stereographic projection between the {111} pole and planes of the <111> zone. Pit sides were found to be {110} planes and edges were in the <110> directions. A chemical etch of dislocations, decorated by the addition of carbon to 50 ppm, revealed the complete dislocation line structure in a surface layer up to 30 μ deep, with a resolution of at lease 1 μ. This effect was independent of surface orientation. Various dislocation structures were noted.

The structure of subboundary nets was resolved up to about 1' misorientation. Dislocation structures such as helices, prismatic loops and high density areas were observed in strain annealed single crystals. This method of chemical etching allows dislocation densities of from 10^5 to 10^8 per sq. cm. to be revealed, these being characteristic of annealed and lightly strained materials. Whereas, transmission electron microscopy is limited to densities greater than 10^8 per sq. cm., because of the small volume of material which can be examined, etch pitting techniques are useful up to dislocation densities of the order of $10^6/cm^2$. Thus an important gap in data acquisition is filled by Vardiman and Achter's method. However, it appears that the method does not work with polycrystalline Nb (present results).

2.2 Microyield

Microyield was originally thought to be a result of dislocation unlocking, movement of dislocations and finally source activation. Van Horne and Thomas (3), while investigating yield and plastic flow in Nb, found evidence which indicates that initial sources of dislocations are located near grain boundaries and precipitates. Evans (1) and Koppenaal and Evans (4) noted that plastic flow is observed in Nb considerably below the σ_{uy} and evidence shows enhanced slip activity near the grain boundaries. This indicates that most dislocation sources are located near the grain boundaries. Evans, using an etch pit technique, concluded that grown-in dislocations do not participate in yielding since they did not appear to rearrange themselves on straining.

It is important to note that it is theoretically possible that the grown in dislocation density may effect the friction stress of a material, and consequently the micro- and macro-yield stresses. This is a result of the work hardening theory relating flow stress and dislocation density, and will be discussed in a later section.

Suits and Chalmers (5) investigated microyielding and yielding in Fe-Si by using an etch pit technique. They found that slip first occurred at the approximate value of the friction stress and single crystal yield stress for silicon-iron, and that it was independent of grain size. As the applied stress was increased more individual grains yielded, and somewhat below the macroscopic yield stress clusters of yielded grains were observed. These latter observations were much dependent on grain size. The percentage of yielded grains at a particular stress was larger in the large grain size than in the fine. Clusters of yielded grains were first seen in the shoulder areas of the samples, indicating that the stress concentration in these areas can promote yield. This was more prevalent in the small grain size than the large, where clusters were observed to form in both shoulder and gauge length. As the stress was increased these clusters formed luders bands and subsequently a yield drop was noted. In the fine grain size the luders band propagated, at constant stress, down the sample gauge length. In the coarse grain size samples the clusters grew quite large in many areas,and the stress at which these clusters coalesced and thereby covered the entire specimen was the lower yield stress. Suits and Chalmers suggested that their results were due to local stress concentrators, such as non-metallic inclusions, which are distributed randomly throughout the matrix. These stress concentrators may act as sources, or may activate sources near them. The following relationship was derived, relating the density of active sources (ρ) to the applied stress (σ).

$$\sigma - \sigma_0 = \frac{k\ m^{-1/n}}{d^{3/n}}\ p^{1/n} \qquad (1$$

where

$$p = m\ d^3\ \rho$$

and where; σ_0 is the friction stress of the material

k and n are constants,

d is the grain diameter,

m is a geometrical constant equal to 1 for cubic grains, and,

p is the probability of a grain having an active source, which is also the percentage of grains yielded,

ρ is the volume density of active sources.

The work of Brentnall and Rostoker (6) deals with the yielding processes in Iron-silicon. Inclusion free material as well as material containing high densities of inclusions were investigated in order to see the effect these differences have on yielding phenomena. Solute atom clusters have been noted in Nb (3) and these may have somewhat the same effect on deformation mechanisms in Nb as inclusions in Fe-Si.

Brentnall and Rostoker (6) found that yielding is a progressive process starting anywhere from 25 to 75% of the lower yield stress. Using etch pit studies on Ni, Fe, and Fe-3% Si they concluded that "the differential between detection of the microyield and macroyield points is least in very coarse grained material and increases with finer grain sizes". Materials that were free from non-metallic inclusions, showed a microyield dependence on grain size when investigated by straining on a tensile machine using strain gauge extensometers of 10^{-6} strain resolution. Etch pitting experiments gave the same result. In samples where high densities of inclusions were present the grain size dependence of the microyield point did not exist. In this latter case, if interpartical spacing was independent of grain size, and if this governs the microyield stress then one would expect a grain size independence.

Brentnall and Rostoker suggested that grain boundaries act as both sources and barriers to slip. Slip, in inclusion free material, was first observed at grain boundaries and was then confined to the mother grain until the upper yield point was reached. In many instances, slip lines eminating from triple points were observed. Since it is unlikely that a band originating in the interior of the grain and ending at a triple point will occur repeatedly, formations of this nature must originate at grain boundary junctions. It was not until the upper yield point was reached that slip activity across grain boundaries was observed. The primary difference, they conclude, between yielding in f.c.c. and b.c.c. materials is the strength of the barrier presented by grain interfaces. In materials containing high densities of inclusions an increase in stress resulted in an increase in etch pit population with no relationship between etch pit arrangements and the grain boundary.

Koppenaal and Evans (4) investigated microstraining in polycrystalline Nb of about four nines purity. Using a load unload technique with a strain sensitivity of 1×10^{-6}, they found that the microyield stress, at that plastic strain, was dependent on grain size, being larger the smaller the grain size. The specimens were then strained to .02074 strain, thereby giving an equal prestrain to them all. This prestrain should produce mobile dislocations in the grains. The microyield stress level was then redetermined by the same technique, and no grain size dependence was found. The new microyield stress was 23 to 32% of that found in the annealed specimens of different grain sizes. These results were explained on the basis that the stress required to move "unlocked dislocations" is much less than that required to release "locked dislocations" from their interstitial atmospheres.

To further investigate locking effects, the same samples were heat treated at 300^{o}C for 16 hours. This recovered the microyield point, but the grain size dependence had been reduced from a difference of 4 kg/mm^2 to about 1 kg/mm^2 for samples of 33 to 450 microns grain diameter. Different thermal treatments will result in different substructure effects and will vary the degree of segregation (or dispersion) of interstitial impurities. Koppenaal and Evans suggested that the grain size dependence of the microyield stress in the annealed specimens reflects the predominating influence of annealing temperatures employed to produce the grain size, rather than a true grain size effect. Prestraining unlocks the dislocations in Nb and the microyield stress recorded in this condition is the lattice friction stress. The same phenomena was found in iron by Ekwall and Brown (7).

2.3 Yield Drop and General Yield

Koppenaal and Evans (4) also investigated macroyielding in Nb by the previously mentioned load-unload technique. Using annealed samples they found that after being loaded to a stress well above the microyield, and subsequently unloading, on reloading the stress rose to a value lower than that previously recorded, and at this stress gross deformation (e.g., 1% strain in a specimen of 33 μ grain diameter) took place. This large strain at a constant stress is indicative of a luders band traversing down the specimen. Although Koppenaal and Evans suggest that the high value of the microyield stress obtained in annealed and strain aged samples is a result of Cottrell (impurity) locking, they do not feel that yielding must be a form of Cottrell unlocking. They suggest that dislocation sources could be created at grain boundaries or other areas of high internal stress and that macroyield is dependent on these.

Van Torne and Thomas (3) show that dislocation unlocking is an unnecessary concept to explain yield drop in Nb. Their data show that yield drop in Nb is accompanied by a large increase in dislocation density, probably through a cross slip mechanism such as described by Low and Guard (8) and Conrad (9). Cross slip may occur at jogs, tangles or subboundaries. It has been fairly well established that any barrier to dislocation motion may be an effective centre for multiplication via a cross slip mechanism. Hirsch (10) has suggested that multiplication can take place at precipitates in this manner. In Van Torne and Thomas's research, the strongest barriers to dislocations for the purities investigated appeared to be solute atom clusters. They propose, therefore, that it is the strong locking effect of barriers which provide the necessary sources for multiplication.

2.4 Grain Size Effects

Most materials exhibit a grain size dependence of the flow stress according to the following relation:

$$\sigma = \sigma_f + kd^{-\frac{1}{2}} \tag{2}$$

where σ_f and k are material constants and d is the grain diameter.

This is commonly called the Hall-Petch relation. Cottrell (11) modeled this equation in terms of dislocation dynamics. Cottrell argued that when the stress concentration at the tip of a pile up reached a certain value, a source inside the unslipped grain would be activated, thus yield would be propagated from grain to grain. From a knowledge of the stress required to activate a source and assuming that the length of the pile up is equal to the grain diameter (d) it was found that:

$$\sigma = \sigma_f + M^2 \tau d\ r^{\frac{1}{2}} d^{-\frac{1}{2}} \tag{3}$$

$$\text{i.e.:}\quad k = M^2 \tau d\ r^{\frac{1}{2}}$$

where M is an orientation factor, τd is the shear stress required to activate a source and r is the distance from the tip of the pile up to the source.

Impurities will affect k if they change the value of τd through pinning. The heavier a source is pinned the higher the stress needed to activate it, thus the larger the value of k. However, experimental evidence indicated that k becomes constant as the ability of a material to pin dislocations increases, and Cottrell's theory does not predict this trend. There is also a lack of direct observation of pile ups in pure metals where the Hall-Petch relationship is valid. A theory which does not require a pile up model was needed. One such theory is the Work hardening theory. Pile ups are disregarded and a linear relation between yield or flow stress and the square root of the dislocation density is taken as an established experimental fact.

Conrad, Feuerstein and Rice (12) investigated the lower yield point and flow stress of Nb, and explained the grain size effect in terms of a work hardening model. They found that the dislocation density was proportional to the reciprocal of the grain size at a given plastic strain, and the dislocation density increased in a linear manner with strain. The tensile flow stress was found to increase with the square root of the dislocation density:

$$\sigma = \sigma_f + \alpha G b \rho^{\frac{1}{2}} \qquad (4$$

where σ_f is the lattice friction stress due to all short and long range obstacles (exclusive of other dislocations) to dislocation motion. α is a constant, and G and b are the shear modulus and Burgers vector respectively. ρ is the dislocation density. σ_f was found to be similar in magnitude to the thermal component of the flow stress of Nb single crystals at 300^{0}K, which has been attributed to the thermally activated nucleation of kinks (13, 14). It is expected that a large part of σ_f is due to this mechanism. Another contribution to σ_f is the impurity content (3). Using their data, Conrad et al, found that $\alpha = .88$. The data of Van Torne and Thomas on Nb yield $\alpha = .84$. These values of α are within the expected range ($\alpha \leq 1$) required by the work hardening models.

Conrad et al (12), found that the increase in dislocation density with strain eventually leads to the development of a cellular network of dislocations. Since the density of dislocations for a given strain increased with decreasing grain size, the smaller the grain size the smaller was the strain at which the cellular network was first well defined. Cell size decreased with strain but at a given strain it was proportional to $d^{\frac{1}{2}}$ (d = grain size). Flow stress was observed to increase linearly with the reciprocal of the cell size.

In general, Conrad et al's results may be summarized in the following relationships:

$$\sigma_{f1} \;\alpha\; \rho^{\frac{1}{2}} \;\alpha d^{-\frac{1}{2}} \;\alpha \frac{1}{L} \;\alpha \frac{1}{l} \qquad (5$$

where σ_{f1} is the flow stress

L is the cell size

l is the average spacing of dislocations based on a random distribution

ρ and d have the usual meanings.

It should be emphasized that the proportionality between cell size and average dislocation spacing is based on the assumption of a random distribution of dislocations.

Another theory relating to the grain size to the flow stress is the grain boundary theory. First proposed by Li (15) and then modified by Li and Chou (16), grain boundaries are assumed to act as sources of dislocations. If "m" is the total length of dislocations emitted per unit area of grain boundary at the time of yielding, then the density of dislocations at the time of yielding is, for a spherical grain:

$$\rho = \frac{1}{2}\,(\pi d^2 m)/\frac{1}{6}\pi d^3 = 3\ m/d \qquad (6$$

where the factor of ½ arises from the fact that each boundary is shared by two grains. Substituting equation 2 into equation 1 gives:

$$\sigma = \sigma + \alpha \; b \sqrt{3m} \; d^{-\frac{1}{2}} \qquad (7$$

which is a Hall-Petch relation with the slope.

$$k = \alpha \; b \sqrt{3m}$$

Tangri, Lloyd and Malis (17) have suggested that grain boundary ledges create stress concentrations large enough to homogeneously nucleate dislocations in the lattice under a small applied stress. Based on this model, Tandon and Tangri (18) have proposed that ledge size may increase with grain size. This may be responsible for some of the variation of the yield stress of Fe-Si, with grain size, since larger grains would yield before smaller ones because of larger stress concentrators in the grain boundary.

Resistance to plastic flow can be measured by hardness. The harder the metal the higher the stress required for plastic flow. This phenomena should also hold true for flow through surfaces, such as grain boundaries. Westbrook, Fliesher, Schodler and Johnson (19) obtained microhardness values of grain boundaries in polycrystalline Nb. Their results showed that with increasing grain size the grain boundary hardness became smaller. This would lead one to expect from some of the current theories of the Hall-Petch relationship that the strength of Nb would increase appreciably as the grain size is refined. This is not normally found as noted by many invesitgations (20, 21, 22, 23, and 24).

Armstrong, Bechtold and Begley (24) suggested that subgrain size may be responsible for the non observance of a grain size dependence in Nb. This implies that subgrain size is the controlling factor for the onset of flow and that this size may not be dependent on grain size. Subsequently the flow stress will not be dependent on grain size. This can only be true if the subgrain boundaries present a greater barrier to dislocation motion than the grain boundaries. The relative strength of the grain or subgrain boundaries could be determined by microhardness tests. Raghuram, Reed and Armstrong (25) set out to see if a hardness gradient did exist across subboundaries, in a single crystal, which would indicate an impurity segregation to those areas. They found a 24% increase in hardness at the boundary over the matrix, i.e. from 37 DPHN to 30 DPHN, with hardness decreasing from the boundary to about 15 μm on either side (crystal surface (211)). The same 24% increase was noted on the Knoop hardness scale on the (111) surface. Westbrook et al's results showed that grain boundaries have three times the hardness exhibited by the subgrain boundaries investigated by Raghuran et al. Therefore in the microyield region flow stress may be dependent on subgrain size. However, during macroyield, flow exists between grains, and the subgrain boundaries should offer little resistance to flow, since the applied stress is at least 3 times that required for flow through the subboundary. Raghuram et al concluded that their results do not give any indication that subgrain is responsible for the grain size independence of the macroyield stresses in Nb.

Omar and Entwisle (26) attempted a study of the effect of grain size on the tensile properties of Nb, in order to make clear the reason for the low and varied grain size dependence of the flow stress, as noted by other researchers. Particular care was taken in the heat treatment of their samples to ensure that contamination did not occur, since various authors have suggested that impurity pickup during the heat treatments were responsible for the low value of k in the Hall-Petch equation. Their specimens were annealed while packed in a zirconium "getter" in a high vacuum. By this method oxygen content was reduced 25%, nitrogen by a factor of 6 and a carbon content of 25 ppm was obtained. In general, they found that the amount of interstitial impurity can be kept constant during heat treatment by using the method described.

Grain diameters from .008 to .25 mm were obtained in .125 mm diameter samples using annealing temperature from 1020^{o} to $1650^{o}C$. A grain size dependence described by:

$$\sigma_{LY} = 4.24 + 1.02d^{-\frac{1}{2}}$$

was obtained for the samples annealed with a getter while in the samples annealed without a "getter", the friction stress changed (from 4.24 kg/ mm^2 to 9.3 kg/mm^2) and k was reduced to zero.

Omar and Entwisle suggest that the above effect arises from contamination with interstitial elements during high temperature treatment in the absence of a "getter"; this results in an increase in σ_f as the annealing temperature is raised to establish the coarser grain size. The net result is an apparent low or zero value of k and a high value of

σ_f.

In brief it has been shown that the grain size independence of the flow stress in Nb may be a result of impurity cluster size and spacing, subgrain size, ledge size variation with grain size and the interstitial impurity content varying with heat treatment. Of these, subgrain size appararently has little effect, interstitial impurity content and "clusters" of impurity atoms may be controlled by thermal treatment, and little is known of ledge size variation with grain size. It is hoped that the present work will determine which of the above governs yielding in Nb.

2.5 Acoustic Emission

Acoustic emission (AE) may be defined as the pressure or stress waves generated in a material due to the energy released by mechanisms that govern its deformation and fracture behaviour (27). Evidence shows that most AE observed from metals can be related to pile up and subsequent breakaway of dislocations as well as from dislocation multiplication, surface effects, and crack propagation (28). All of these constitute a release of energy in the lattice. Tangri, Toronchuck and Lloyd (27) summarized the mechanisms which can give rise to AE and ranked them in order of the amount of energy released. They conclude that dislocations, in free flight, give rise to very low amplitude emissions. Dislocation breakaway will give slightly larger ones and the largest will occur from pile up breakaway and source generation of dislocations.

Tandon and Tangri (18) investigated AE during deformation of polycrystalline silicon iron. Using both etch pit and AE techniques they studied the dislocation processes which occur at various strain levels. The amplitude of AE signals (events) were found to be of the same magnitude in both the micro and macroyield regions. Etch pitting revealed much source activity from the area of grain boundaries in the microyield region. This should be the main source of AE in this regime and as such, is expected to release approximately the same amount of energy each time it operates. In the macroyield region, dislocation pile ups serve to enhance stress concentrations at the grain boundaries, and result in further grain boundary generation. This process is commonly referred to as "pile up breakaway". Since generation by grain boundary sources is the most prevalent form of deformation in the micro and macroyield regions, no change in AE event amplitude is expected.

Tandon and Tangri found that in the work hardening region both AE activity (events per unit time or rate) and amplitude were low. This is explained by the low energy generated by the dislocation mechanisms operating in this region, and by the relatively constant value of the mobile dislocation density. Tandon and Tangri noted some medium sized events in this region and attributed them to pile up and multipole breakaways. They also noted that small grain sizes showed a slightly larger amount of AE activity than the large grain sizes in the work hardening region. Since dislocation networks and substructures are smaller in the small grain sizes, then one would expect a larger number of the above two mechanisms and hence enhanced AE activity.

AE rate, is defined as the number of events recorded in a specific time interval. Tandon and Tangri found a higher total event count (ΣN)

in coarse grain sizes in the microyield region. It was assumed that if grain boundary ledge sizes increased and thus stress concentration increased, with an increase in grain diameter, then the number of sources activated at a particular stress would be greater in larger grain sizes. The results of Suits and Chalmers (5) support this view since the number of slip lines per grain as well as the fraction of yielding grains increase at a faster rate in coarse grained material as opposed to the finer grained.

In the macroyield region the above trend is reversed, the AE activity increasing with smaller grain sizes. This is due to the fact that dislocations in a coarse grain sized sample can take up a higher proportion of strain than one in a fine grain sized sample, since they can slip a larger distance before being stopped by the opposite grain boundary. Thus smaller grain sized samples require the creation of larger numbers of dislocations to match the constant strain rate imposed upon them by the instron machine. Since the rate of dislocation multiplication increases the AE activity increases.

In summary, Tandon and Tangri concluded that the AE technique could be used as a valuable tool in the study of the dynamical nature of deformation, and that a good correlation exists between dislocation mechanisms and observed acoustic emission.

3.0 Experimental Techniques

3.1 Materials and Sample Preparation

The material selected was 3 mm thick sheet of 99.9% pure Nb, supplied by Wah Chang, Albany. The ingot analysis supplied by the manufacturer is shown in Table 1.

Two sets of tensile samples were prepared. In the first set, sample blanks were cut from the sheet stock and were cold rolled 50% except those designated for the smallest grain size which were rolled 66%. A tensile-cut machine was used to cut samples with a 2 cm gauge length. Each sample was mechanically polished on numbers 166, 320, 400 and 600 metallographic papers, then chemically polished in 25% HF - 75% HNO_3 for 1.5 minutes at room temperature. Final thickness of the samples ranged from 1.2 to 1.4 mm. The specimens were then sealed in 19 mm vicar tubing which was then purged with commercially pure Argon 3 times, drawing a vacuum of approximately 10^{-5} torr between each purge. The tube was then sealed at 150 torr Argon. Mechanical and thermal treatments and the resulting grain sizes for sample set 1 are shown in Table 2. After removal from the furnace the samples were allowed to cool in the tube to room temperature. A final homogenizing treatment at 800^{o}C for 1 hour was given to all samples.

Sample set 2 was prepared using a slightly different technique than set 1, namely; grain size was controlled by prior cold rolling and not by varying the annealing temperature. This new technique was used for two reasons;

Analysis in PPM		
Element	Top	Bottom
Al	<20	<20
B	<1	<1
C	<30	<30
Cd	<20	<20
Cd	<5	<5
Co	<10	<10
Cr	<20	<20
Cu	<40	<40
Fe	<50	<50
H	5	<5
Hf	<50	<50
Mg	<20	<20
Mn	<20	<20
Mo	<20	<20
N	10	35
Ni	<20	<20
O	<50	110
Pb	<20	<20
Si	<50	<50
Sn	<10	<10
Td	<100	114
Ti	<40	<40
V	<20	<20
W	12	17
Zr	<100	<100

TABLE 1

INGOT ANALYSIS (WAH CHANG ALBANY)

Grain Size	Preparation*	Size (±15 μ)
1	66% deformation 980°C 1 hr.	38 μ
2	50% deformation 998°C 1 hr.	83 μ
3	50% deformation 1040°C 2 hrs.	95 μ
4	50% deformation 1200°C 2 hrs.	258 μ
5	50% deformation 995°C 1 hr. 2% deformation 1200°C 24 hrs.	466 μ

TABLE 2

PREPARATION OF SAMPLE SET 1 SPECIMENS

Grain Size	Preparation*	Size (±15 μ)
21	60% deformation 1100°C 1 hr.	-90 μ
22	40% deformation 1125°C 1 hr.	-138 μ
23	50% deformation 1200°C 1 hr.	-168 μ
24	35% deformation 1200°C 1 hr.	-214 μ
25	25% deformation 1200°C 1 hr.	-195 μ
26	15% deformation 1200°C 1 hr.	-305 μ

TABLE 3

PREPARATION OF SAMPLE SET 2 SPECIMENS

*final treatment to all specimens - 800°C 1 hr. air cooled.

1. by varying the amount of prior cold work, the desired grain sizes could be produced at a relatively constant annealing temperature. This ensures that impurity pick up will be constant between the various grain sizes. This would, hopefully, minimize the effect of the picked-up impurities on the grain size dependence of the yield stress.
2. In the case of large grain sizes, thicker specimens were used in order to ensure a minimum of five grains in the cross section. This serves to reduce the specimen size effect reported by Conrad et al (12).

The polishing and sealing procedures were the same for this set as for sample set 1. Table 3 gives the details of the rolling and heat treatments for set 2. Following the annealing treatment each tube was removed from the furnace and immediately given a homogenization treatment at $800^{o}C$ for 1 hour, then air cooled.

3.2 Polishing and Etching

Electro polishing and etching were done in a solution of 15% HF - H_2SO_4 at a temperature of $30\text{-}40^{o}C$ using a graphite anode. For the etch pit studies, the samples were electropolished for 15 to 20 minutes at approximately 6 volts. (Current density decreases with electrolyite used, and is therefore not a good indication of the polishing conditions). Etching was accomplished at 1 volt for 1 minute, followed by 15 seconds at about 1.5 volts; this removed reaction products from the specimen surface. The specimen was immediately washed in water and then ethanol.

3.3 Grain Size Measurement

For the purposes of this study, grain size or grain diameter is defined as the average distance from a grain boundary to the next nearest grain boundary as measured along a randomly placed straight line on an exposed plane of the sample. The method of determining grain size was the random intercept method. A number of random lines were drawn on 20 photomicrographs of each grain size and the number of grains, N, in a given length, l, was determined. The grain size is given by:

$$d = \frac{l}{mN}$$

where m is the magnification.

3.4 Dislocation Density Measurement

Dislocation density may be defined as the number of intersections dislocations make with a plane of unit area.

Twenty grains were chosen in each sample. Care was taken so that these were representatives of the sample and that their average grain size would closely match that found by the intercept method. Etch pit density was determined by the formula:

$$E_\rho\,(\mathrm{cm}^{-2}) = \frac{\text{Average number of Etch pits per grain}}{\text{Average Area of grains } (\mu^2)} \times 10^8$$

Schoeck (29) has shown that the actual dislocation density (ρ) should be:

$$\rho = 2(E\rho)$$

where the factor 2 is brought into correct for orientation effects.

Since only comparative values are of interest in this work it was assumed that $E\rho = \rho$, i.e., the etch pit density is equal to the dislocation density.

3.5 Mechanical Testing

The object of these experiments was to determine the characteristics of the microyield region in polycrystalline Nb. Two series of tests were carried out.

3.5.1 Step-loading

Specimens from sample set 1 were decoration treated at $300^{o}C$ for 16 hours in tantalum foil, then etch pitted to reveal any signs of dislocation generation due to handling. Each sample was strained to 3.1 kg/mm^2 in an Instron machine at a strain rate of 4.17×10^{-4}/sec. The machine was stopped at the above strain and after one minute the load was taken off the sample. Each sample was then decoration treated, electropolished and etched again. Notes and photographs were taken of any slip line activity. Specimens not showing slip line activity were stressed again, the stress being increased by 1 kg/mm^2 over the previous value. The process was repeated until definite evidence of slip line activity was noted in all samples. At 3.1 kg/mm^2 the smallest grain size showed no slip lines but did show a definite increase in dislocation density. After this stress the samples were pulled past the lower yield point. This was done because the samples were becoming very thin ($\sim$ .5 mm), as a result of the repeated polishing treatments, and the risk of handling deformation was too great.

The same step loading procedure was done for 2 specimens (85 and 394 μ) of grain diameter sample set 2, except that the strain rate was changed to 8.34 x 10^{-5}/sec. to allow greater control of loading. After each load step, dislocation density and slip line density were recorded and photographs were taken of any interesting deformation characteristics as exhibited by etch pits.

3.5.2 Load Cycling

Four specimens from sample set 1 were fitted with strain gauges. The grain sizes tested were 260, 258, 85 and 97 μ. Figure (1) shows that strain was measured via an Accudata-218 bridge amplifier with output to a Hewlett Packard x-y recorder. The 260 and 85 μ samples were pulled in an Instron machine at a strain rate of 1.67 x 10^{-5} sec^{-1}, strain could be resolved to 25 μ strain. The 258 and 97 μ samples were pulled at the same strain rate but the step-loading technique was used. Strain was resolved to 6.25 μ strain.

Care was taken when performing the load cycling tests to ensure that the specimen was accurately centered along the load axis. The longitudinal axis of the specimen was aligned with the load axis of the Instron by using the special grip system strain in Figure (1). Pins and precision measured "spacers" were used to obtain the correct alignment of the axis. By knowing the grip system geometry and dimensions, and also the specimen thickness, the appropriate "spacers" could be inserted in the system to ensure alignment. The tolerances achieved in the machining of the grip system and spacers ensured that the load axis and sample axis were at all points within .1 mm from each other.

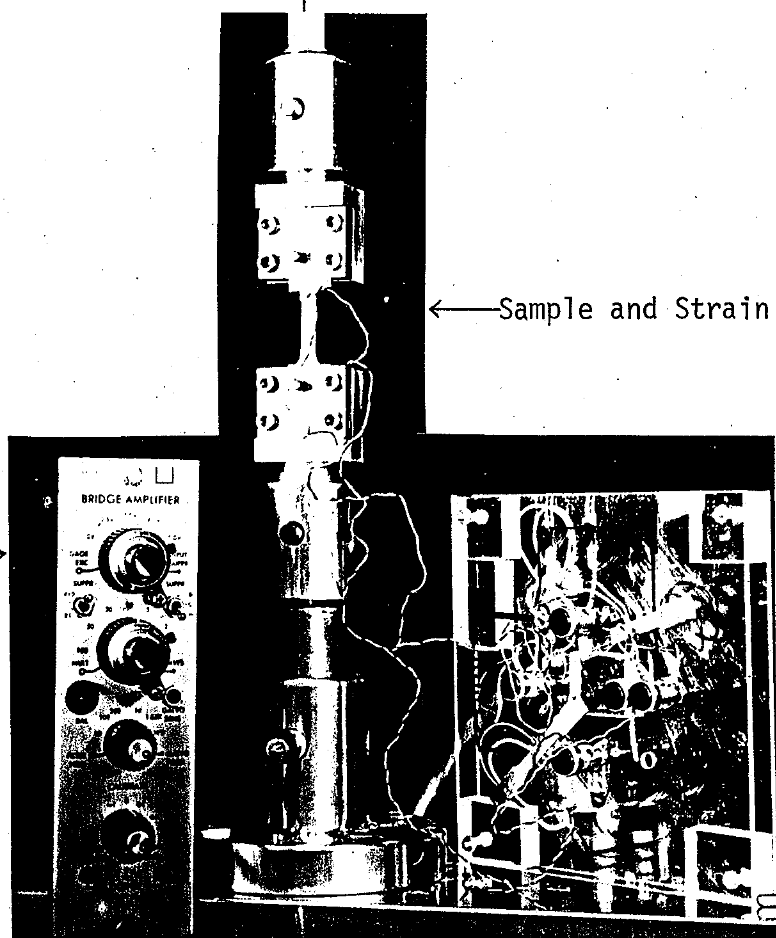

Figure 1: Apparatus used for Load Cycling Tests

The microyield stress was defined as that stress which gave the specimen a plastic strain of 6.25×10^{-6} as recorded after the stress had been removed. After microyield the load-unload tests were continued into the macroyield regions.

3.6 Etch Pit Studies

Although detailed etch pit studies were included in the tests for microyield determination and characteristics, it was decided to investigate etch pit patterns at the upper and lower yield points also.

Four specimens of sample set 2 were chosen, 96, 147, 225 and 300 μ. The samples were electropolished smooth and strained in an Instron machine until the upper yield point was just observed and then unloaded. They were then treated for 16 hours at 300^{0}C in Tantalum foil, electropolished and etch pitted. Photographs were taken of all interesting features. The samples were then electropolished again and strained into the luders region, and the process of polishing, etching and analysis repeated.

3.7 Acoustic Emission Tests

The acoustic emission (AE) record and playback block diagrams are shown in Figures (2) and (3). Appendix I gives a detailed account of the equipment's function and operating procedure.

3.7.1 Sample Preparation

Two sets of AE tests were completed. The first used specimens from sample set 1. To avoid extraneous noise which may be created by the common clamp type of grip system during loading, a system involving only pins passing through the sample grip section was evolved. This system is

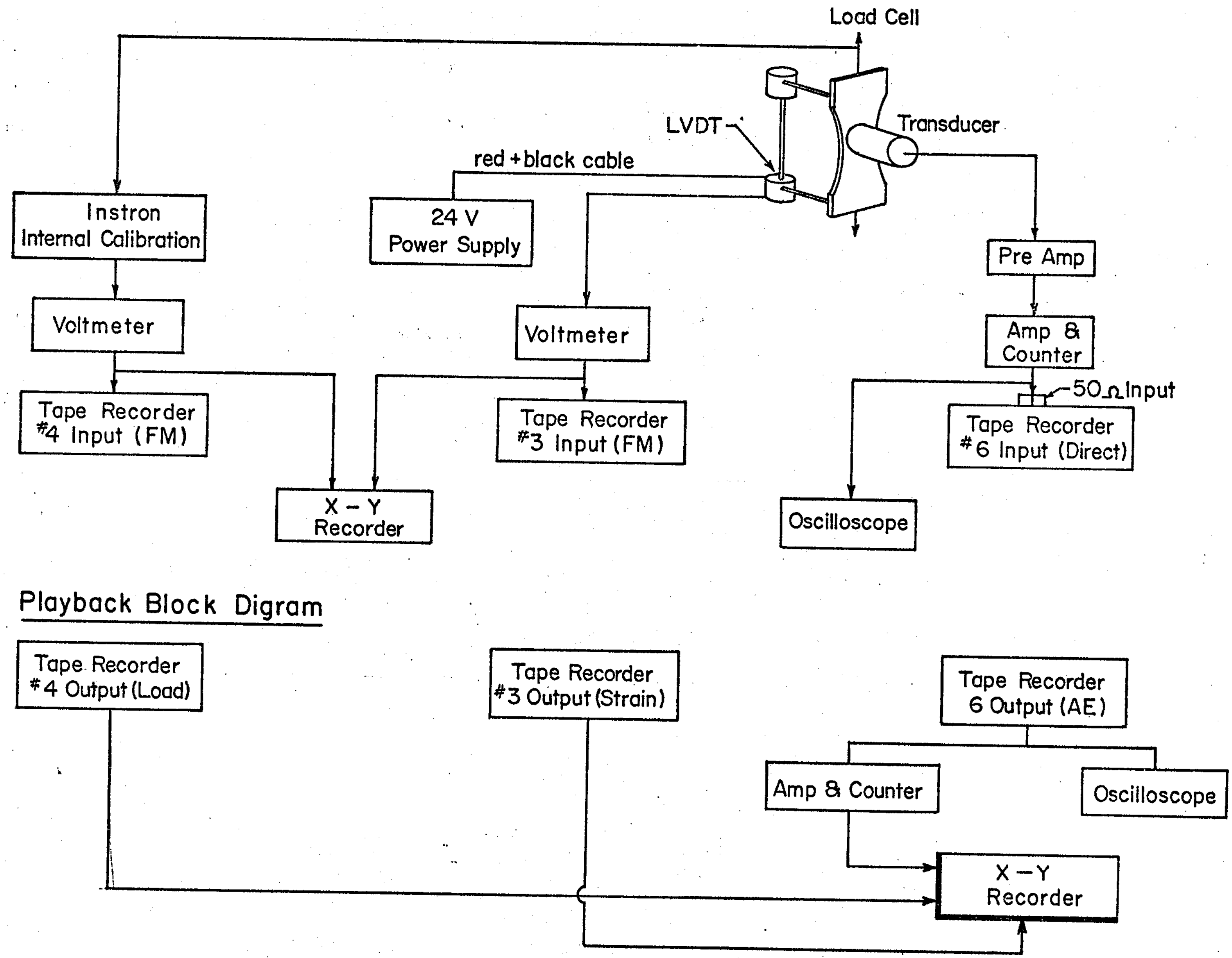

Figure 2: Acoustic emission recording and playback system.

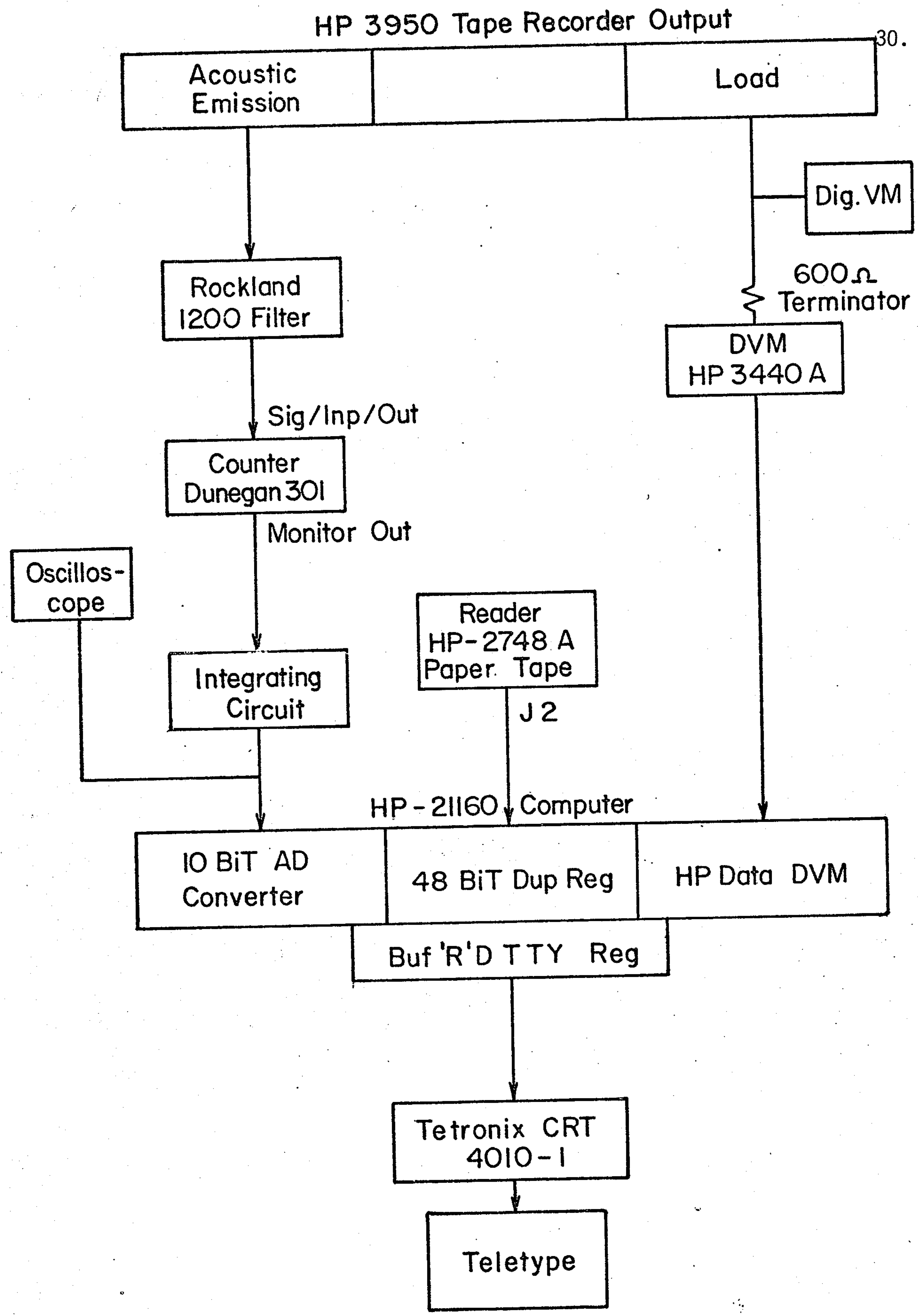

Figure 3: Acoustic Emission Analysis System.

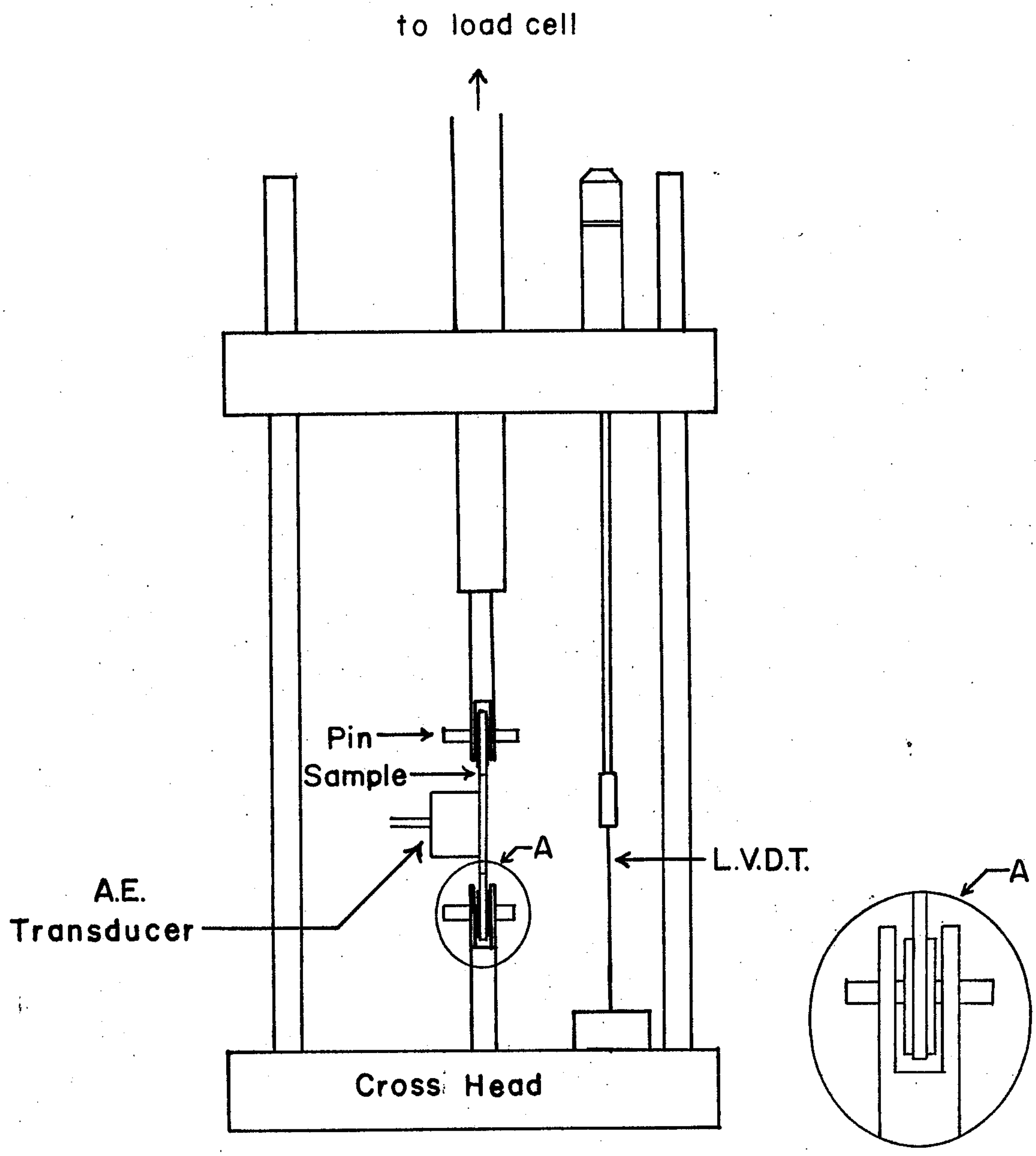

Figure 4: Detail of Grip System used for Acoustic Emission Tests on Sample Set 1.

shown in Figure (4). Stainless steel reinforcing pads were glued onto the grip sections of the samples with Aerobond type 2125 cement and cured for one day at room temperature. These reinforcements should reduce the load carried by the material near the pin thus preventing any extraneous noise from entering the system due to plastic deformation from the sample area in contact with the pin.

Of course, the cement may crack as strain is placed on the sample. From previous results obtained in this laboratory, this does not usually happen until approximately 7 to 10% plastic strain, and any cracking of the glue was easily recognized on the AE output signal, thus AE from the glue can be ignored or the sample and results can be rejected from the test series.

Using a special jig, holes were drilled through the reinforcement pads along the axis of the sample. During the drilling some of the pads cracked off the samples. This was thought to be due to the compressive stress placed on the grip section by the drilling jig, and the shear stress applied by the drill bit. The pads (about 25% of them) subsequently fell off after removal from the drill jig. They were then cleaned and recemented to the sample taking special care in lining up the holes, and finally cured for the recommended time. The specimen to be tested was attached to the Instron machine by means of pins, and a LVDT set up so as to record strain.

The second set of AE tests used sample set 2. These samples were prepared in a slightly different manner than set 1 owing to the difficulties encountered with the reinforcing pads. No reinforcing pads were used with

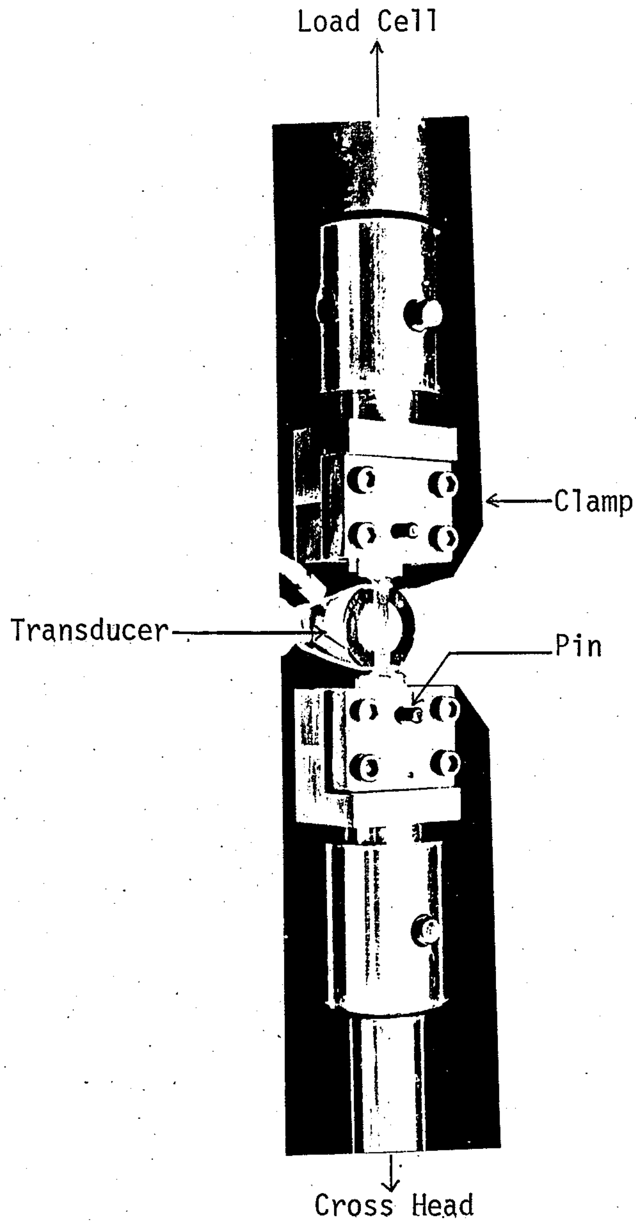

Figure 5: Grip system used for acoustic emission tests on Sample Set 2

set 2 and the grip system was changed to that of Figure (5). In this system pins were used to align the specimen with the tensile axis of the machine, while serrated clamps were used to transfer the load to the sample. The sample pins and clamps were assembled in an alignment jig, and while in this jig the clamps were compressed onto the sample with a load of about 400 kg/cm^2 at the sample grip section and the clamps were tightened. This should work harden the grip sections of the sample and no AE activity is expected from these areas until the gauge length of the sample is well within the work hardening region. (This is making a practical use of the Kaiser effect). This system had one disadvantage; it was not possible to have an LVDT measurement of strain, instead of time base was used.

3.7.2 Test Conditions

In preparation for tests on sample set 1, the magnetic tape was calibrated for the LVDT, AE and load channels as outlined in the Appendix. The strain rate was set at 4.17 x 10^{-4}/sec. and the transducer was attached to the specimen using vacuum grease as a transfer medium and an elastic band for mechanical support. The transducer used in these experiments was the Endevco Corporation model number S9201 with PZT-5 sensing elements. It responded to motion normal to its surface and had a frequency response of .1 to 1.0 Mhz at -76 db.

Electrical noise in AE recording and analysis was eliminated by the use of an electronic "trigger" which essentially eliminated all signals below a certain voltage. In the present work noise created within the electrical system was eliminated by the ability to control the cut off voltage (trigger level) via a variable gain amplifier. Electrical noise resulting from outside electrical disturbances and variations in line voltages, if above the trigger level, were not controlable. However, these were monitored before each test via an oscilloscope. Typically over a period of 5 minutes, 1 or 2 small spikes would be observed. Considering that each AE test was approximately 3 minutes long, and consisted of as many as 700 events or as few as 250, it was determined that outside electrical disturbances were insignificant both in frequency of occurrence and amplitude for the purposes of this study.

The gain level of the amplifiers was set at 76 db. Specimens were pulled under these conditions and the stress, strain and resulting AE recorded. Recording and loading were stopped after about 7% deformation. The results were then analysed as described later.

Testing conditions for sample set 2 were identical to 1 except in three areas. (1) The specimen grip system was as described in the previous paragraphs. (2) The recording level was set at 82 db since this was found to be the level where the largest events in Nb would not overload the system (the counter rejects any signal greater than 10 volts) and yet the background noise level was just below the trigger level of the counter. (The counter rejects any voltage below 1 volt). (3) The AE tape channel was calibrated to 7 volts peak to peak instead of 5 volts as in set 1, to ensure that peak amplitude up to 7 volts (the maximum expected from the results of set 1) would be recorded.

3.7.3 Analysis

Analysis of both sets of AE experiments was performed on the Hewlett Packard 2118C Computer. The program was designed to calculate and record the emission or count rate per second, the sum of total "counts" from the beginning of the test, the average amplitude of the emissions in each second, and the peak amplitude which occurred during each second.

The signals from two grain sizes (87 and 305 μ) from sample set 2 were further investigated in detail by using a Biomation Waveform recorder. Individual events were "captured" by the recorder in various stages of deformation. The recorder is able to sample a signal at a rate of 1×10^7 samples per second, giving a total record length of .205 m sec. According to the Niquist theorem, this sampling rate enables an accurate description of frequency to be made up to 5 Mhz. The frequencies expected in this study were 60 to 750 khz; well below the maximum that could be recorded. Using the above mentioned settings on the Biomation recorder it was found that signal amplitudes were accurate to within 5% at 400 khz with a 10 volt peak to peak signal. An attempt was made to find the major frequency component of the captured signals by counting the signal's peaks over a time period and dividing by that time interval.

4.0 Results

4.1 Etch Pits in the Microyield Region

Figure 6 shows that the grown in dislocation (etch pit) density (ρ_0) increases with decreasing grain size, and that it is independent of the two types of thermal-mechanical treatments employed in this study. It should be noted however, that dislocation etch pitting is to some extent, orientation dependent in Nb. Thus the experimental values of the dislocation densities in Figure 6 are likely to be an underestimate, while the profile of the curve is not expected to be significantly in error.

Figures 7 and 8 show that both fine and coarse grain sizes exhibited an inhomogeneous grown in dislocation distribution.

Most grains had areas in them having a larger ρ_0 than the balance of the grain. These regions were more prevalent in the finer grain sizes than in the coarse ones. Coarse grain sizes exhibited some subboundaries as shown in Figure 8a.

Figures 9 and 10 show typical examples of the first evidence of slip activity. The fine grain size (Figure 9) shows only an increase in etch pit density which is not readily seen from the photograph. Larger grain sizes, such as that in Figure 11, show a slight increase in general dislocation density plus slip bands which often traverse completely across the "parent" grain, and sometimes promote slip in the adjacent grain as shown in the regions about "A" in Figure 10. It is emphasized that even though some bands appear to end at a grain boundary, the adjacent grain may be orientated in such a way that the continuing band is not etch pitted and therefore not visible in the photograph. Subboundaries do not appear to impede the passage of slip bands, as noted at points "B" in Figure 10.

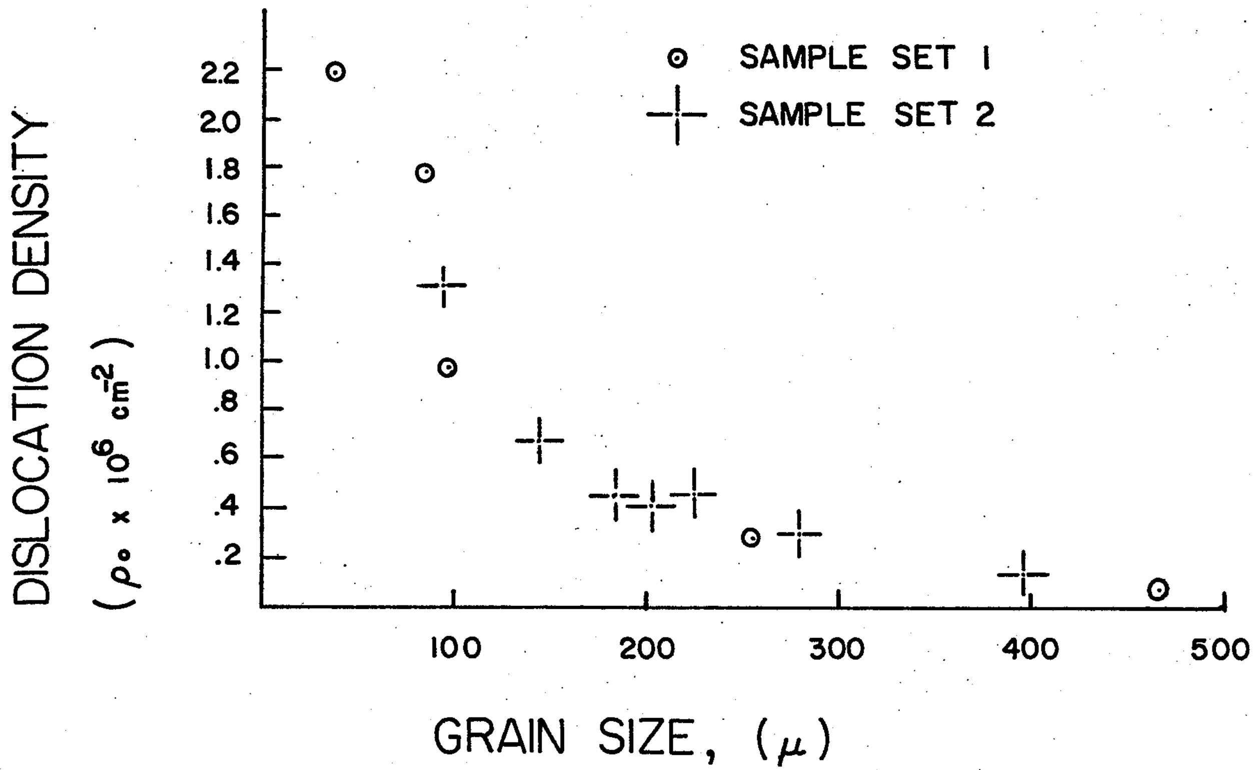

Figure 6; Grown in Dislocation Density vs. Grain Size.

(a)

(b)

Figure 7: Annealed Structure of an 85μ Grain Diameter Specimen

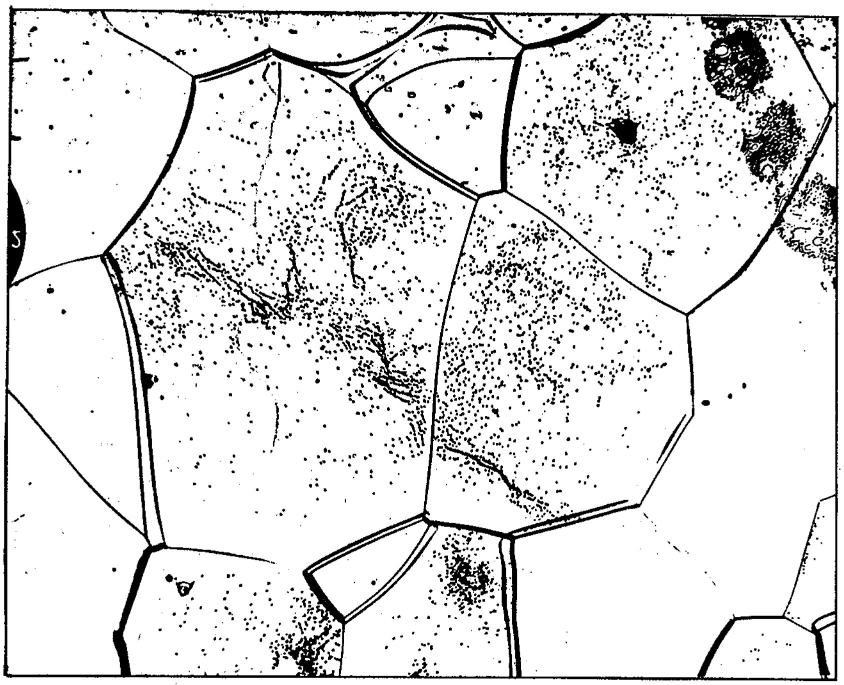

(a)

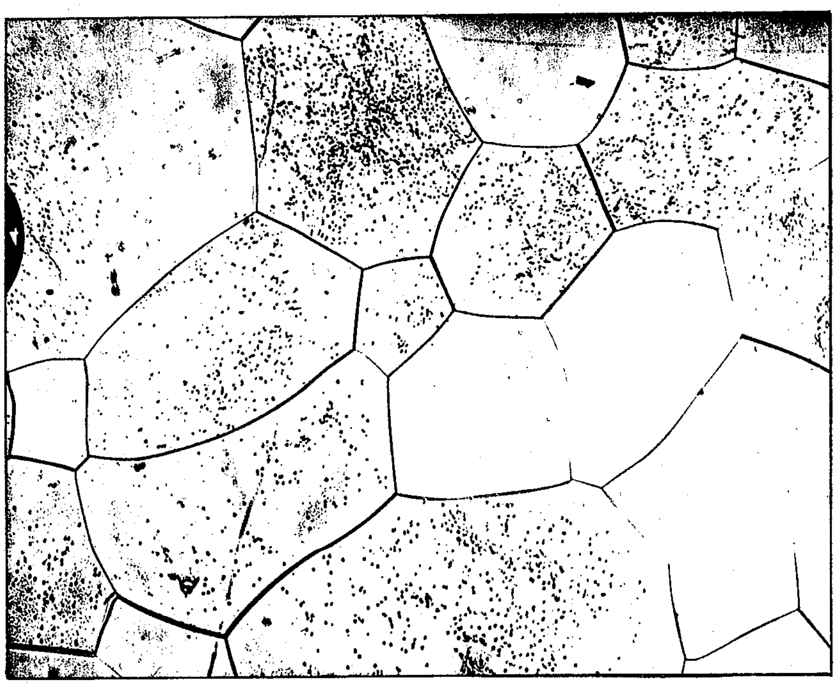

(b)

Figure 8: Annealed Structure of Larger Grain Sizes; a) 305μ (104X)
b) 200μ (143X)

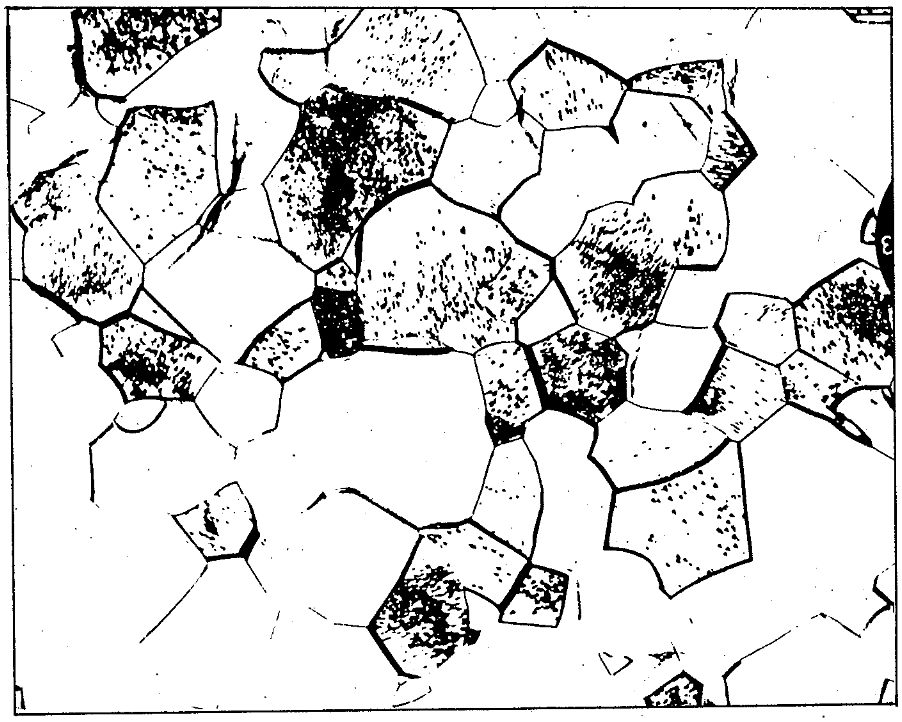

Figure 9: 80μ Sample at 40% σ_{ly}. (130x)

(a)

(b)

Figure 10: 305μ Sample at 40% σ_{1y}. (104x)

This supports Raghuran et al's (25) results which indicate that subboundaries are not formidable barriers to slip propagation in Nb. In coarse grained material, as the stress is increased, dislocation sources generate greater numbers of slip bands. Figure 11a and b show a number of slip bands at 67% σ_{ly} in the coarse grain size. Most bands appear to originate at grain boundaries as a row of etch pits (slip lines), as noted at "C" in Figure 11b. However, some bands were noted to exist in the middle of some grains, neither beginning nor ending at a grain boundary ("D" in Figure 11a). Slip lines such as these may be the result of dislocation sources located in the grain interior.

Slip lines did not appear in the fine grain sizes until about 76% σ_{ly}. Figure 12a and b show the first observed slip band activity in an 80μ specimen. Grains such as those marked "G" contain many slip bands and slip lines. Slip across grain boundaries occurs often.

At 80% σ_{ly} the coarse grain size material shows many slip bands and areas of very high dislocation density as shown in Figure 13a and b. Slip bands are noticeably broader than those observed at lower stresses, indicating that cross slip of dislocations is taking place. Areas near some grain boundaries appear to have very high dislocation densities such as those marked "F" in Figure 13.

At the upper yield point the fine grain size (Figure 14a and b) show broad slip bands, slip propagation across grain boundaries, and a few grains with very large dislocation densities. Groups of grains near the shoulders of the specimen had extremely large dislocation densities.

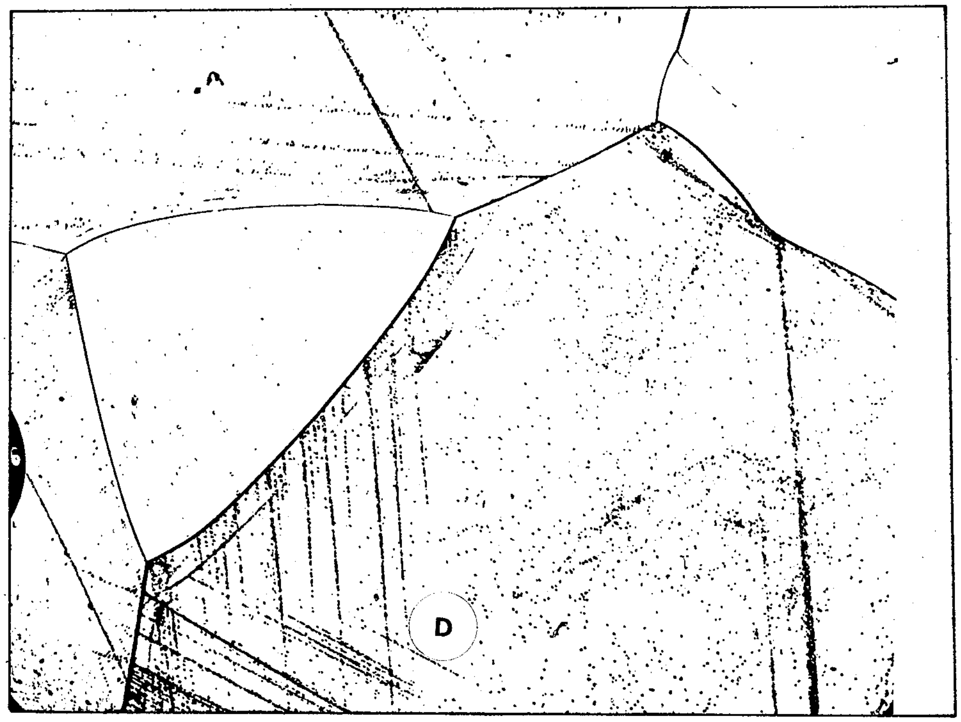

(a)

(b)

Figure 11: 305μ Sample at 67% σ_{ly}. a) 390x b) 85x

(a)

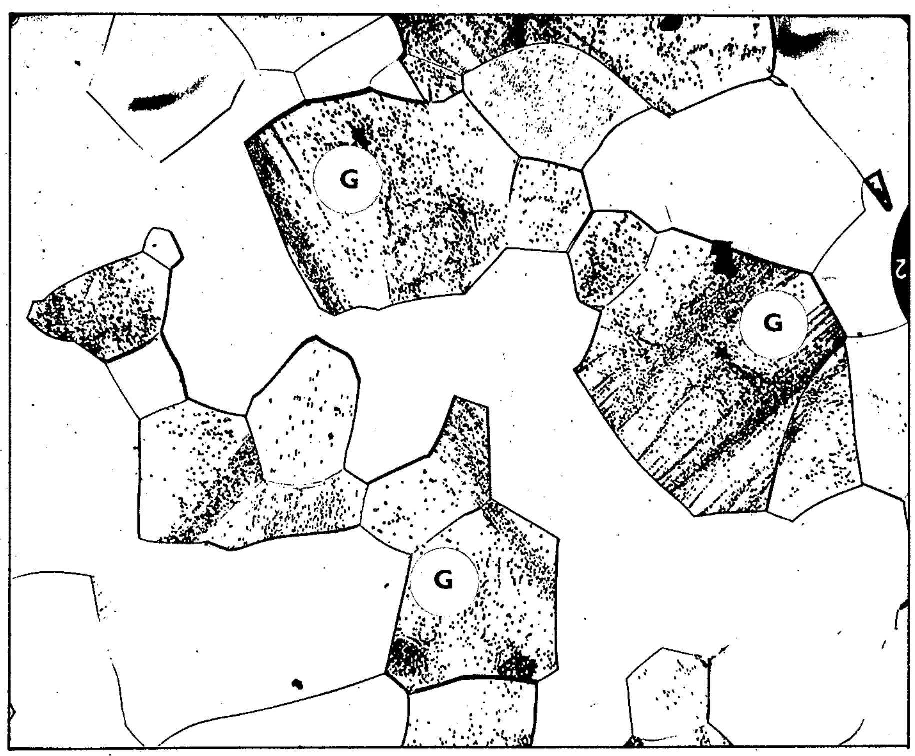

(b)

Figure 12: 80μ Sample at 76% σ_{1y}. (150x)

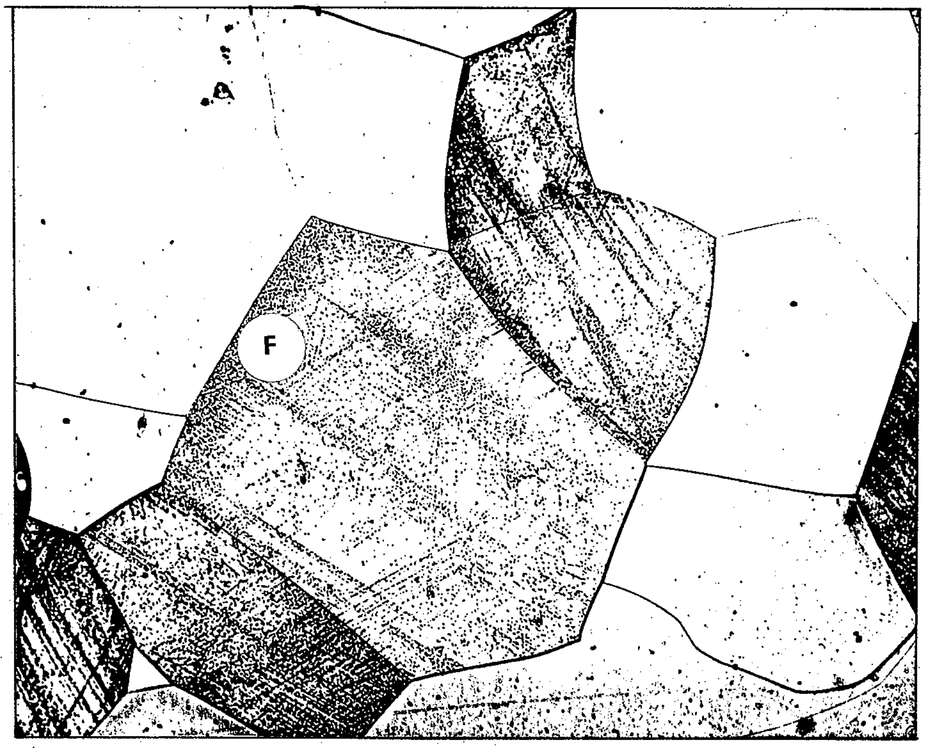

(a)

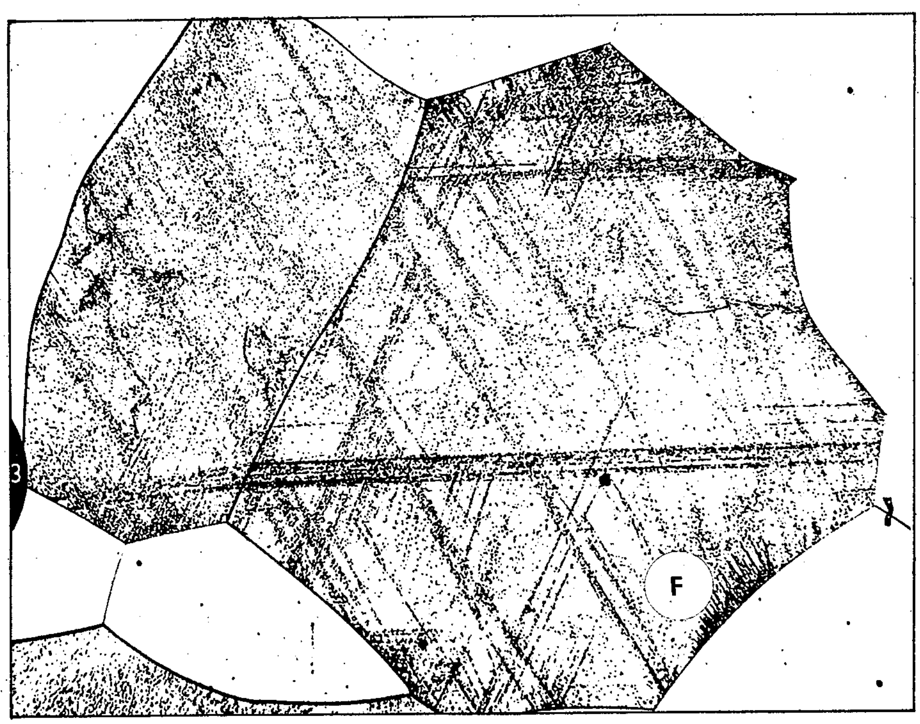

(b)

Figure 13: 305μ Specimen at 80% σ_{ly}. (100x)

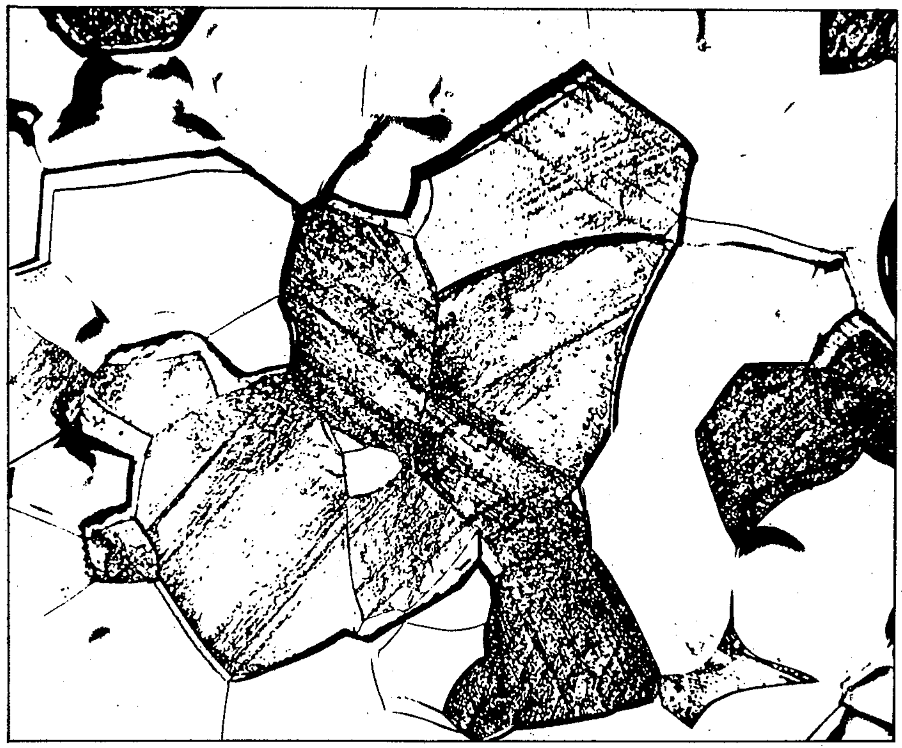

(a)

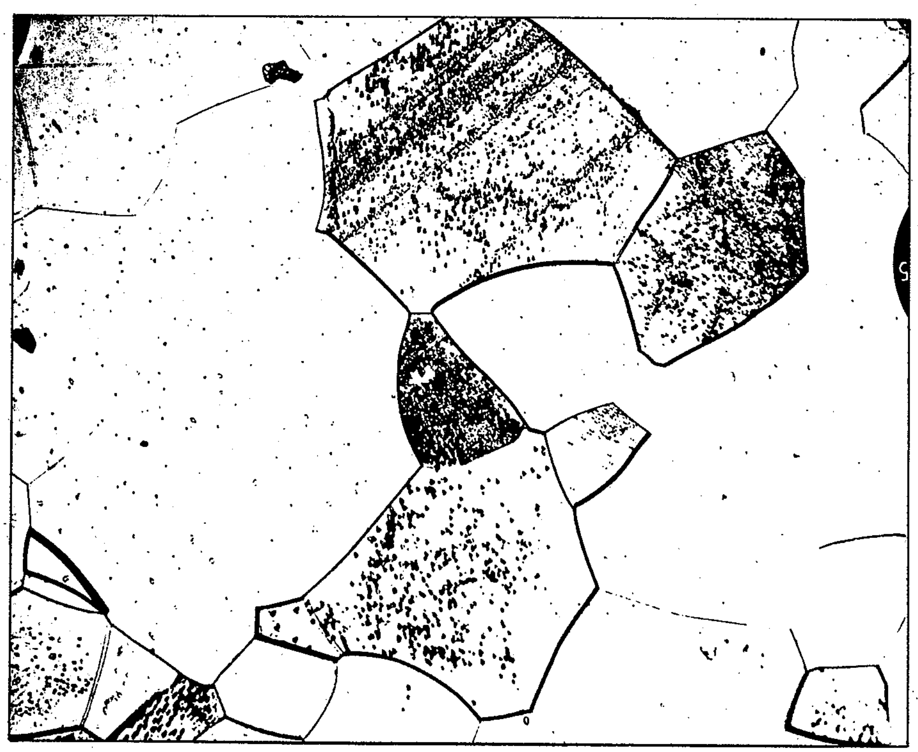

(b)

Figure 14: 80μ Sample at the upper yield stress. a) 143x b) 182x

The coarse grain size at the upper yield point stress, Figure 15a and b, exhibited large dislocation densities, much slip across grain boundaries, and broad slip bands.

Near area "H" in Figure 15a, a slip band has acted as a barrier to slip and created several dislocation pile ups. This phenomena was observed in many grains. As in the fine grain size, the coarse exhibited groups of grains near the shoulders of the specimen which had extremely large dislocation densities.

On further straining in both coarse and fine grain sizes, the highly deformed grains near the specimen shoulders appear to initiate the Lüders band. The Lüders band propagates across the width of the specimen then propagates down the gauge length at relatively constant stress. Figure 16 shows a series of photographs taken across a Lüders band front in a 147μ grain diameter specimen. "J" indicates the region where the Lüders front has just passed, leaving highly deformed grains to the right of "J". The front moves to the left and as a relatively undeformed grain comes under the influence of the band, greater numbers of slip bands are formed in it, and these bands broaden as the Lüders front approaches. Eventually etch pits fill the grain becoming unresolvable at "J". It appears from etch pits that cross slip is the major mechanism of dislocation multiplication in the Lüders region.

The diffuseness of the Lüders band was approximately the same in all grain sizes, being about 1.2 mm. At least two bands were formed in each specimen. Nuclei were initially formed at each end of the gauge length near the specimen shoulders, and a third band was sometimes observed

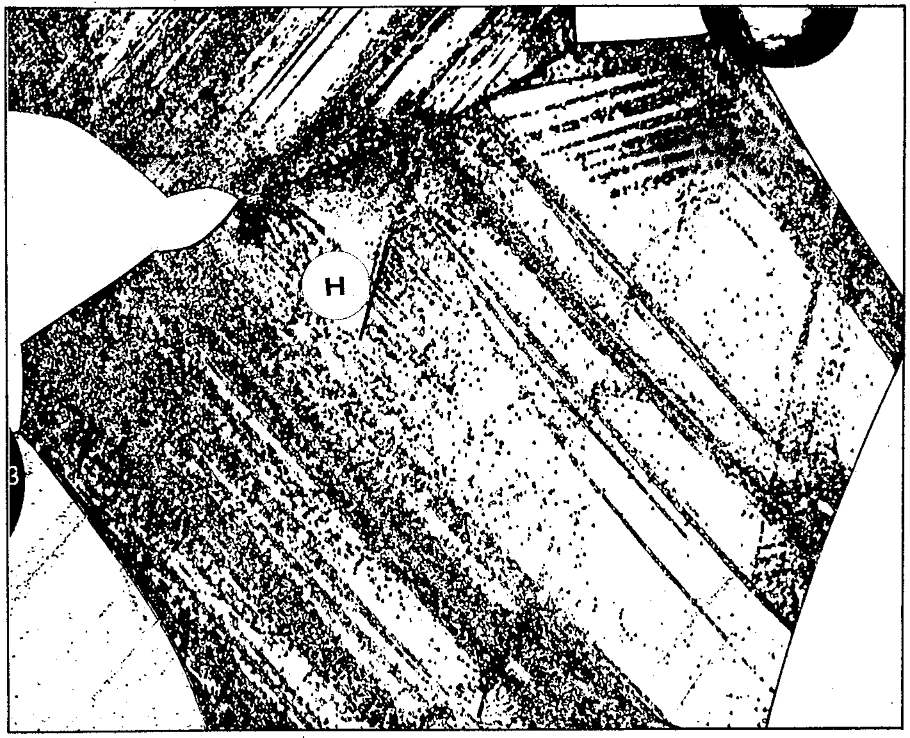

(a)

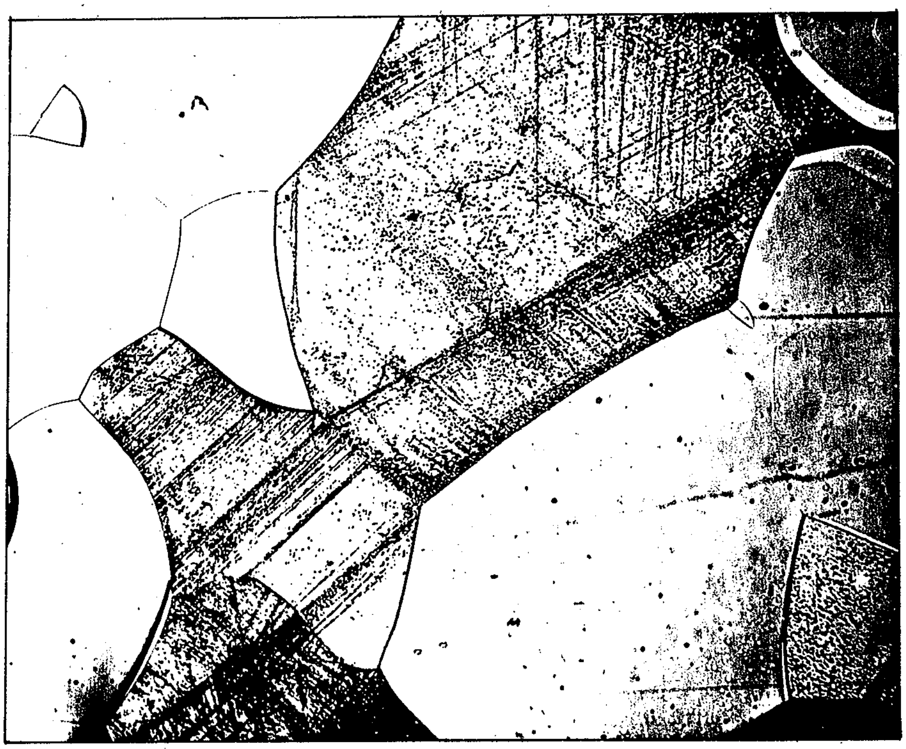

(b)

Figure 15: 305μ Sample at the Upper Yield Stress. a)208x b)95x

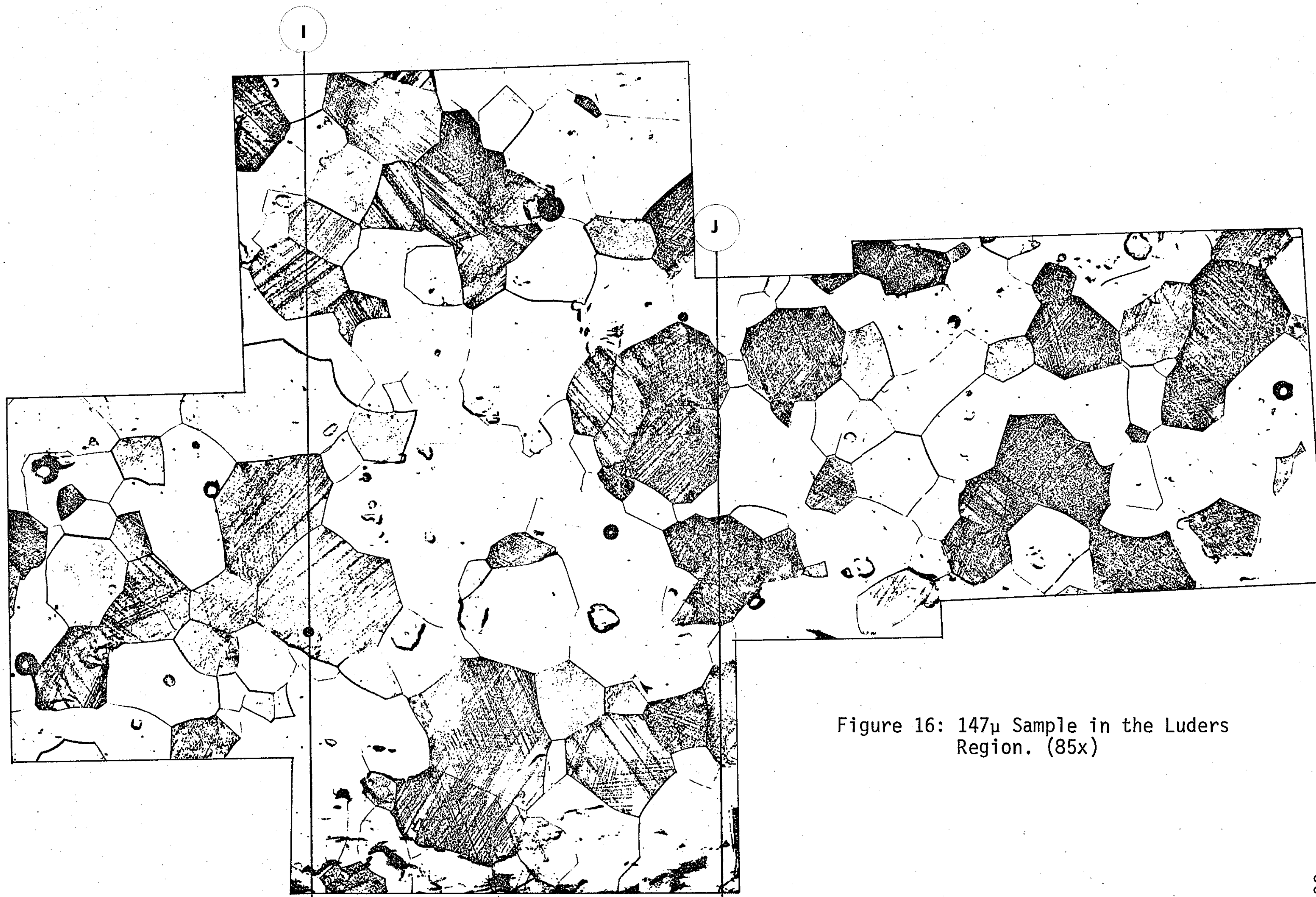

Figure 16: 147μ Sample in the Luders Region. (85x)

in the gauge length probably resulting from a particularly severe stress concentration in that area.

Once the Lüders band had covered the whole specimen gauge length, the samples entered the work hardening region of the stress-strain curve and the stress began to rise. Plastic deformation in the work hardening region has to be the result of the interaction and multiplication of dislocations within the grains.

4.2 Micro and Macroyield Stresses

Figure 17 shows a plot of true stress as a function of $D^{-\frac{1}{2}}$ (i.e., a Hall Petch plot) at various strains. σ_i represents the stress at which dislocation activity was first observed by etch pits. Note that σ_i is independent of grain size and occurs at about 3 kg/mm^2. σ_{S1} is defined as the stress at which slip bands were first noted in the specimens, and it is grain size dependent, increasing as grain size decreases. In the largest grain size tested, σ_i and σ_{S1} coincide, indeed σ_i was determined for this grain size by the formation of slip bands as well as by a small increase in dislocation density outside the slip band areas. In fine grained samples an increase in ρ was the first indicator of σ_i, no slip bands were noted until higher stresses, i.e., σ_{S1} were reached, hence the σ_{S1} and σ_i lines diverge in Figure 17.

σ_{my} is the stress at 6.25 x 10^{-6} plastic strain. It increases with grain size as noted in Figure 17 and may be described by:

$$\sigma_{my} = .5 + .64\ d^{-\frac{1}{2}}$$

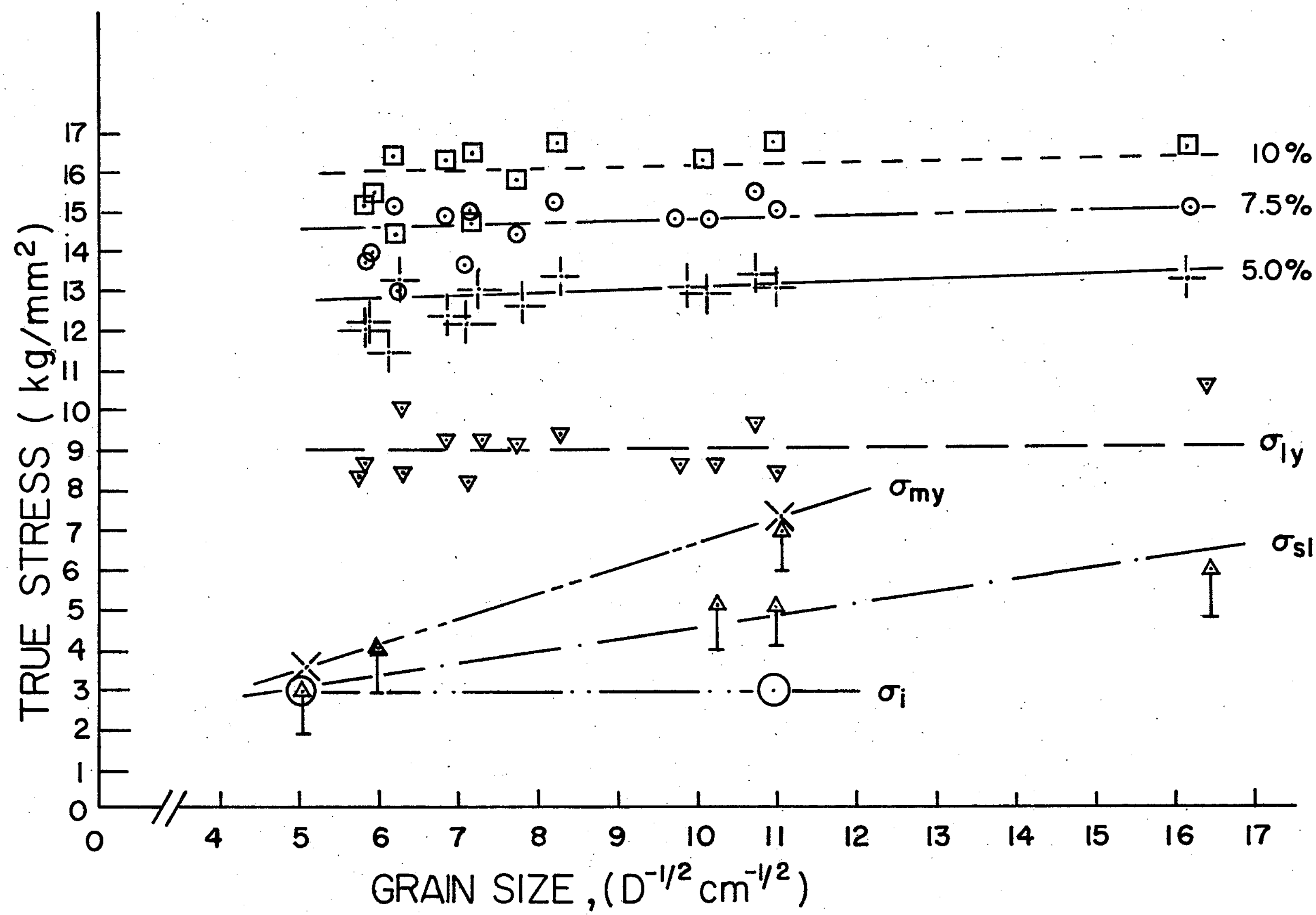

Figure 17: Hall-Petch Plot of True Stress vs. $D^{-\frac{1}{2}}$ at Various Strains.

Somewhat after the microyield the specimens showed an upper yield point, a Lüders region and a work hardening region. Of importance to this work is that the lower yield stress (σ_{ly}) and the stress at 5, 7.5 and 10% plastic strain showed no significant variation with grain size.

Figure 18 shows the dislocation density not including the dislocations in slip bands, as a function of the stress in percent of σ_{ly} for 2 grain sizes. The data points of 0% σ_{ly} represent the grown in dislocation density of the annealed specimens. Between 0 and approximately 40% σ_{ly} the data lines are dashed indicating that uncertainty exists as to where ρ begins to increase.

At 40% σ_{ly} the coarse grain size forms slip bands and no increase in ρ outside these bands was noted, hence the curve is a straight horizontal line. The fine grain size shows an increase in ρ at 40% σ_{ly} with a relatively homogeneous dislocation distribution. Hence the curve representing the fine grain size slopes sharply from 40% σ_{ly} to higher dislocation densities as the stress increases.

Table 4 shows the dislocation density, percent of grains with slip bands, and the average number of slip bands per grain at various percentages of the lower yield point.

4.3 Load Cycling Experiments

Figure 19 and 20 show load versus strain diagrams for the load unload experiments conducted on two grain sizes. As noted in Figure 19 a 97μ specimen was loaded to stress "A" and at that point the crosshead motion was reversed, and the load removed until about 5 kg remained on

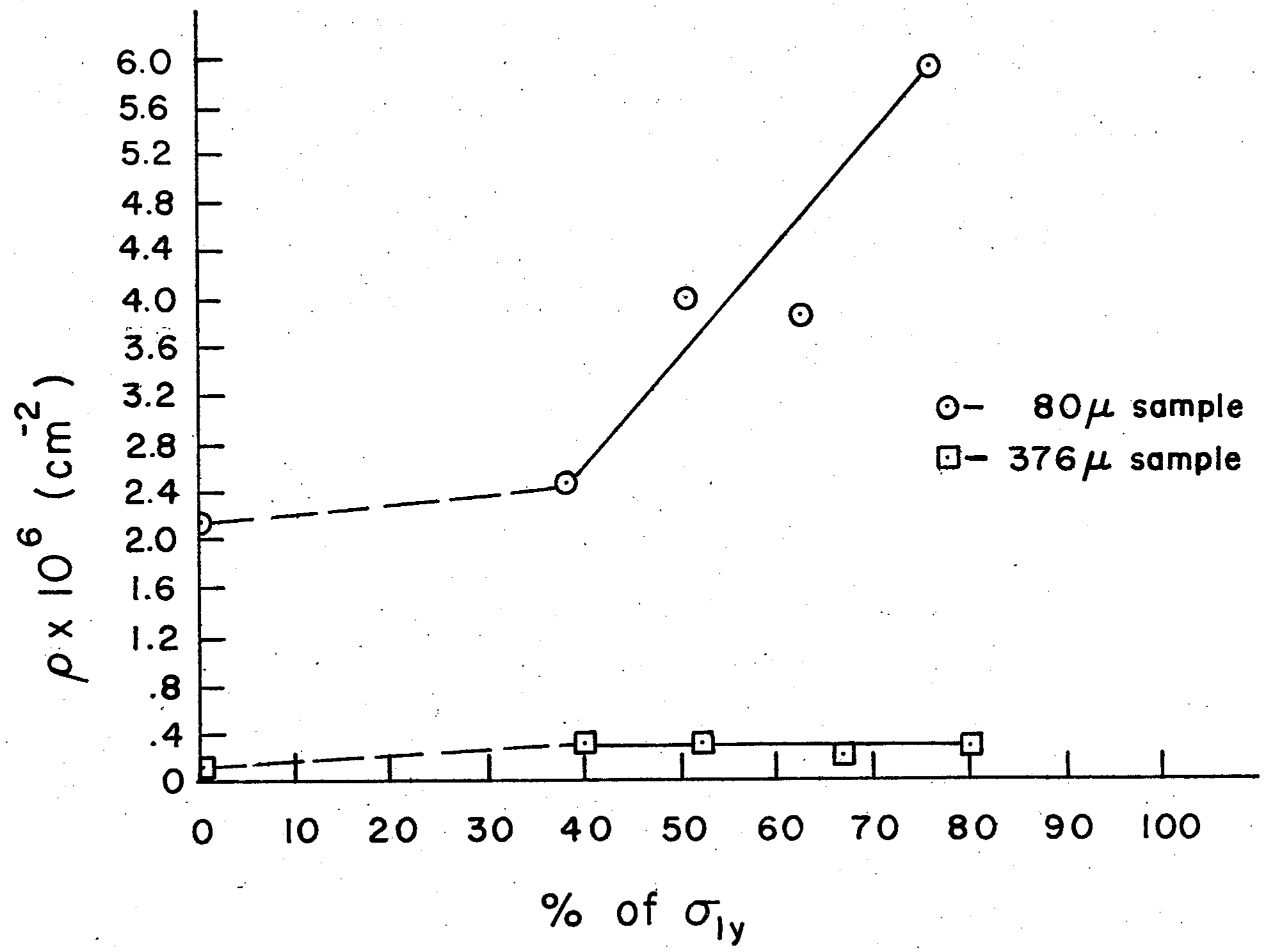

Figure 18: Dislocation Density, not including Dislocations in Slip Bands, in the Microyield Region vs. Percent of the Lower Yield Stress.

% Lower Yield	0	38	51	63	76	Uyp
$\rho(x10)^{6\dagger}$	2.20	2.46	4.06	3.81	5.90	1500
% Grains with Slip Bands	0	0	0	0	62	All
Average No. of Slip bands/Grain	0	0	0	0	Many*	

GRAIN SIZE 80 μ

% Lower Yield	0	40	53	67	80	Uyp
$\rho(x10)^{6\dagger}$	.16	.24	.24	.21	.23	72.5
% Grains with Slip Bands	0	26	43	-	-100	All
Average No. of Slip bands/Grain	0	2.15	3.5	-6	Many*	

GRAIN SIZE 376 μ

TABLE 4

RESULTS OF STEP LOADING AND ETCH PIT EXPERIMENTS ON 2 GRAIN SIZES

---

†Does not include dislocations in slip bands.
*Individual slip bands not resolvable.

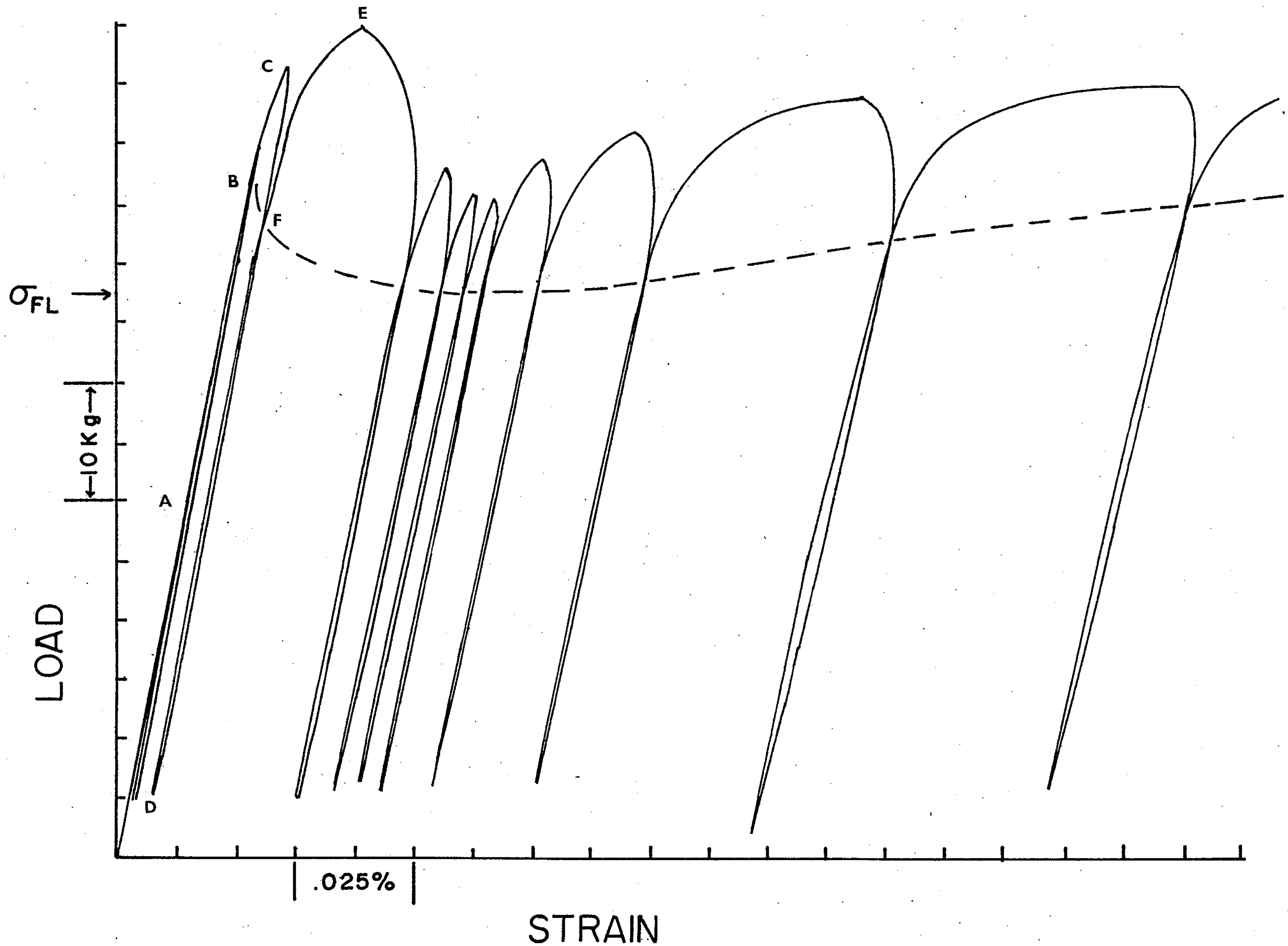

Figure 19: Load vs. Strain from Load Cycling Tests on a 97μ Sample, Sample Area=8.36mm^2.

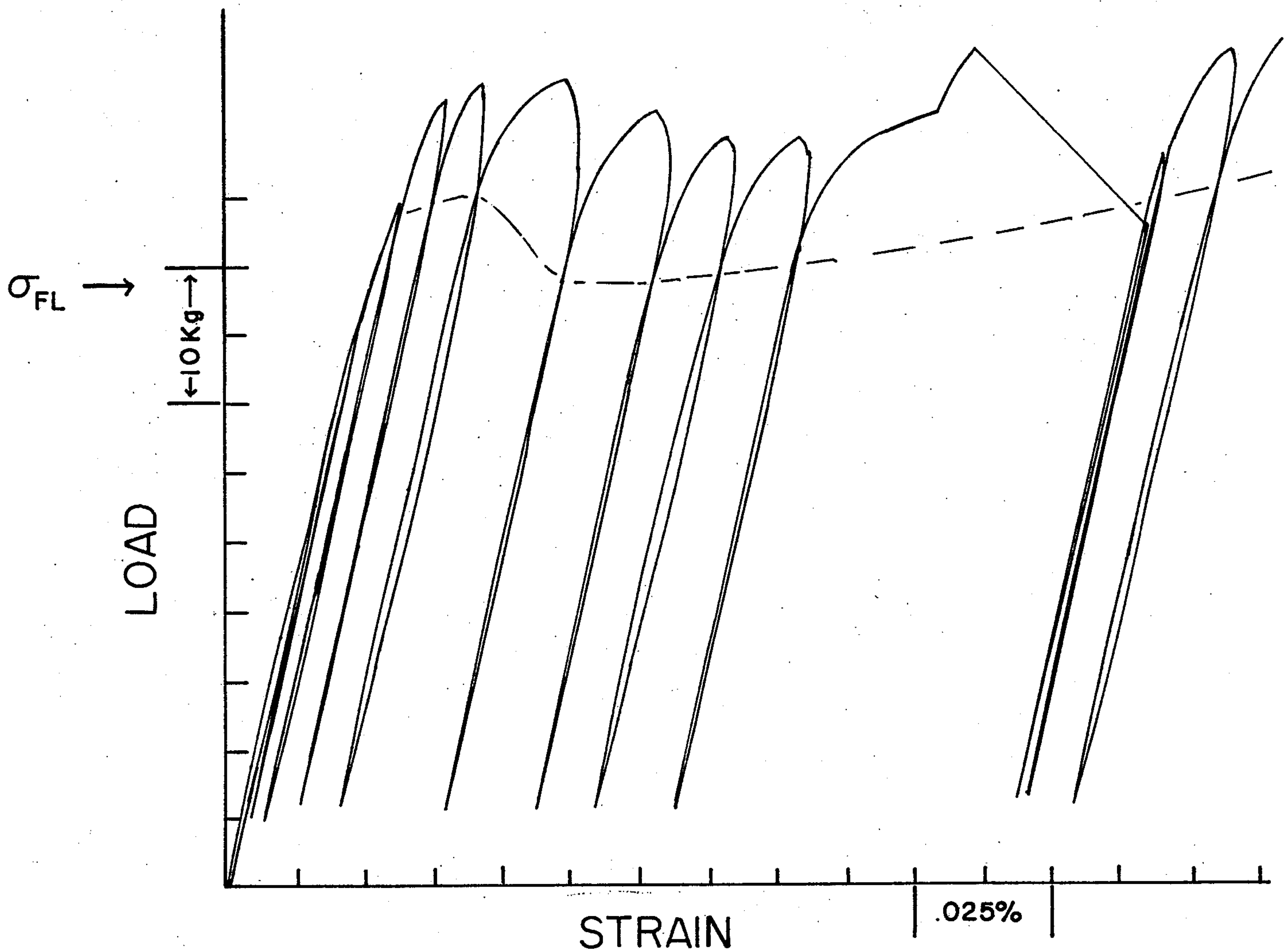

Figure 20: Load vs. Strain for Load Cycling Tests on a 258μ Sample, Sample Area= 7.93 mm^2.

the specimen. No residual plastic deformation was noted. The cycle was repeated three times, the maximum stress being increased for each cycle past that stress reached during the previous cycle. After loading to point B and unloading a permanent strain of approximately 6×10^{-6} remained, therefore the stress at point B was called σ_{my} as noted earlier. The specimen was then reloaded to C and unloaded to D. On reloading from D to E a point F was reached where the unload C-D curve was crossed by the loading D-E plot. F approximately indicates the stress where the sample begins to deform plastically during the D-E loading curve, i.e., it is an indication of the onset of flow after cycling to a plastic strain of about .0625%. For each stress cycle after σ_{my} a point such as F exists. The dashed line in Figure 19 and 20 joins all these points. This line gives a good indication of the minimum stress required to promote plastic flow in the material at various strains.

Figure 21 shows the nominal stress strain curves for samples much the same as those tested in the load cycling experiments.

Table 5 gives the pertinent information that was found from both the load cycling and nominal stress strain experiments.

4.4 Acoustic Emission

4.4.1 General

Figures 22 and 23 show the AE output from two typical specimens as analysed by the Hewlett Packard 2118C computer: "A" indicates the load curve, "B" shows the total count curve, "C" shows the count rate curve

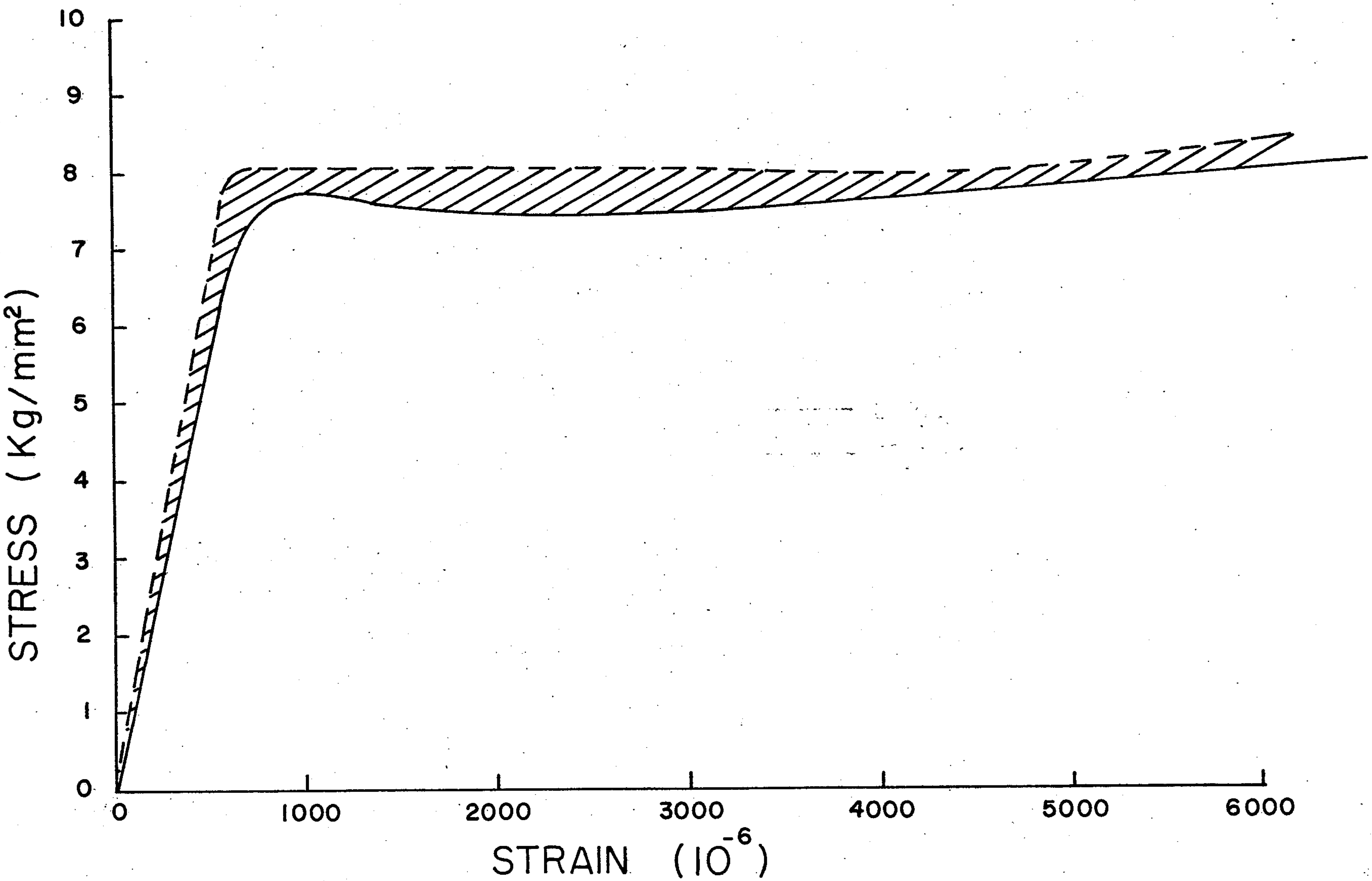

Figure 21: Approximate Range of Test Results for Specimens Strained with Strain Gauges.

Data from Stress-Strain Curves of Figure 21			Data from Load Cycling Test of Figures 19 & 20		
Grain Size	260 μ	85 μ	Grain Size	258 μ	97 μ
Strain Rate	1.67×10^{-5} sec^{-1}			1.67×10^{-5} sec^{-1}	
σ_{uy} (Kg/mm^2)	7.78	8.07	σ_{uy}	-	-
Yield Drop (Kg/mm^2)	.34	.112	Yield Drop	-	-
σ_{Ly} (Kg/mm^2)	7.44	7.96	σ_{FL}	5.49	5.71
Lüders Strain	.175%	.375	-	-	-
Youngs Mod. (Kg/mm^2)	1.06×10^6	1.08×10^6	Youngs Modulus	1.98×10^6	2.14×10^6
σ_{my}* (Kg/mm^2)	6.1678	7.29	σ_{my}**	3.46	7.21
Work hardening rate Kg/mm^2	205	279	Work hardening rate†	336	423

TABLE 5

MECHANICAL PROPERTY DATA FROM TESTS USING STRAIN GAUGES

*Based on 12.5×10^{-6} strain offset

**Based on 6×10^{-6} strain.

†Found from continuation of test without cycling.

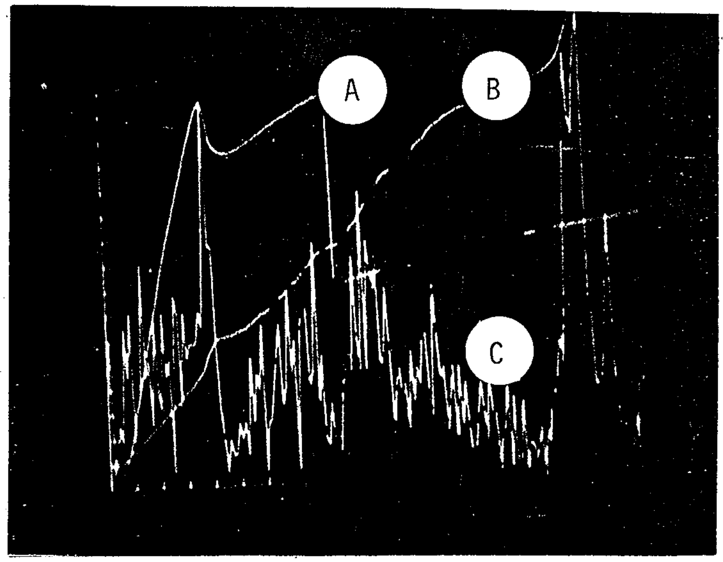

a) 'A' -Load, 100→ 200 kg. = Full Scale.

'B' -Total Counts, 1000 Counts = Full Scale.

'C' -Count Rate, 25 Counts/Second = Full Scale.

x axis -Strian, 180 Seconds= 7.5% Strain = Full Scale.

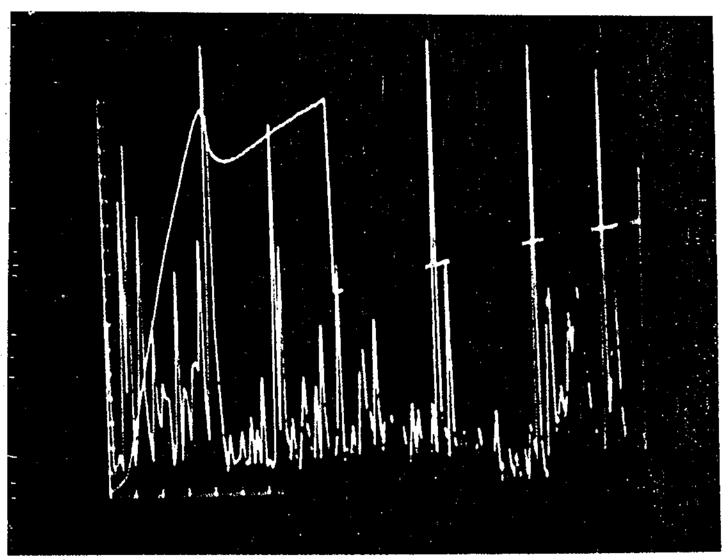

b) Peak Amplitude -y axis= 500μv = Full Scale.

Figure 22: Acoustic Emission Results of 83μ Sample.

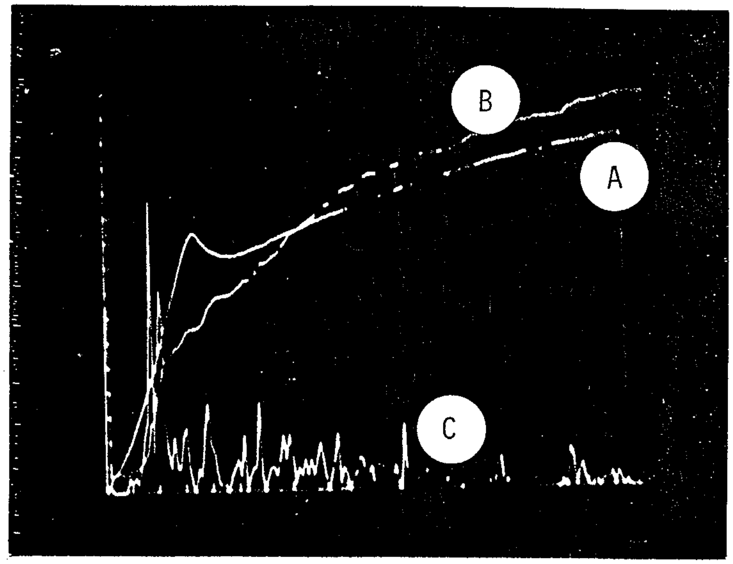

a) 'A' -Load, 200 kg. = Full Scale.

'B' -Total Counts, 500 Counts = Full Scale.

'C' -Count Rate, 50 Counts/Second = Full Scale.

x axis -Strain, 180 Seconds= 7.5% Strain = Full Scale.

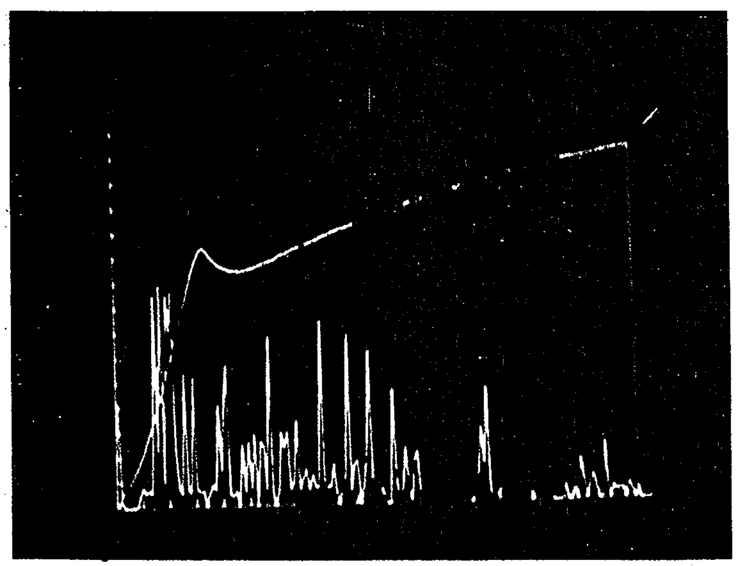

b) Peak Amplitude -y axis= 1000μv = Full Scale.

Figure 23: Acoustic Emission Results of a 290μ Sample.

as plotted against time.

In the fine grain size acoustic emission began at the onset of straining as shown by the count rate curve in Figure 22a. A moderate AE rate was noted until just before the upper yield point, where relatively large count rates were observed. During the yield drop AE rate decreased to about 20% of that at the upper yield point and remained at that value until just inside the work hardening region. As straining continued the rate began to rise and reached moderate values at 3 to 4% strain and then began to decrease again. The very large count rates near the end of the test shown in Figure 22a is thought to be extraneous noise resulting from the slipping of the grips which attach the specimen to the Instron machine.

Figure 22b shows the peak amplitude of the pulses in each one second interval of the test. The load curve is also plotted for easy reference. Moderate to large amplitudes are noted in the microyield region, but the emissions with the largest amplitude are found in the yield drop area. The Lüders region contains very low amplitude pulses, while during the work hardening region a few very large amplitude emissions occur.

The results of the coarse grain size are depicted in Figure 23a and b. Acoustic emissions occur almost immediately on loading, and the count rate rises rapidly to its peak value at about 50% of σ_{ly}. The rate then decreases to a relatively low value and remains there throughout the rest of the test. The peak amplitude per unit time (Figure 23b) follows the same pattern, the maximum value being in the microyield region, with smaller peaks occurring throughout the remainder of the test. An occasional large peak amplitude was noted in the Lüders and work hardening region.

4.4.2 Acoustic Emission Grain Size Dependence

Figure 24 and 25 show how the total number of emissions during the microstrain and Lüders region varies with grain size for the two sample sets tested. Figure 24 shows the results from Sample Set 1. The trigger level was set at 79.4μv (i.e., signals below 79.4μv were not taken into account) because the noise level of the equipment was found to be just below that level. Figure 25 shows the results for Sample Set 2, where due to noise problems with the equipment, the trigger level had to be set at 158μv.

Even though testing conditions of the two sets of experiments differed, they show the same trends. In the microyield region the number of counts increased as the grain size was decreased and the total emission counts in the Lüders region did not vary significantly with grain size.

Figures 26, 27 and 28 show plots of the average and peak amplitude of emissions. Figure 26, up to the upper yield stress, Figure 27, from the upper yield stress to 2.5% strain, and Figure 28, during the work hardening region from 2.5% to 5% strain. The 2.5% strain level was chosen to ensure that the Lüders band had completely passed through the samples, and that work hardening had begun.

It appears from this data that no relationship exists between grain size and acoustic emission pulse amplitude.

4.4.3 Acoustic Emission Signal Analysis

A somewhat limited signal analysis was carried out on 20 individual pulses from 2 grain sizes in the three regimes of the stress strain curve.

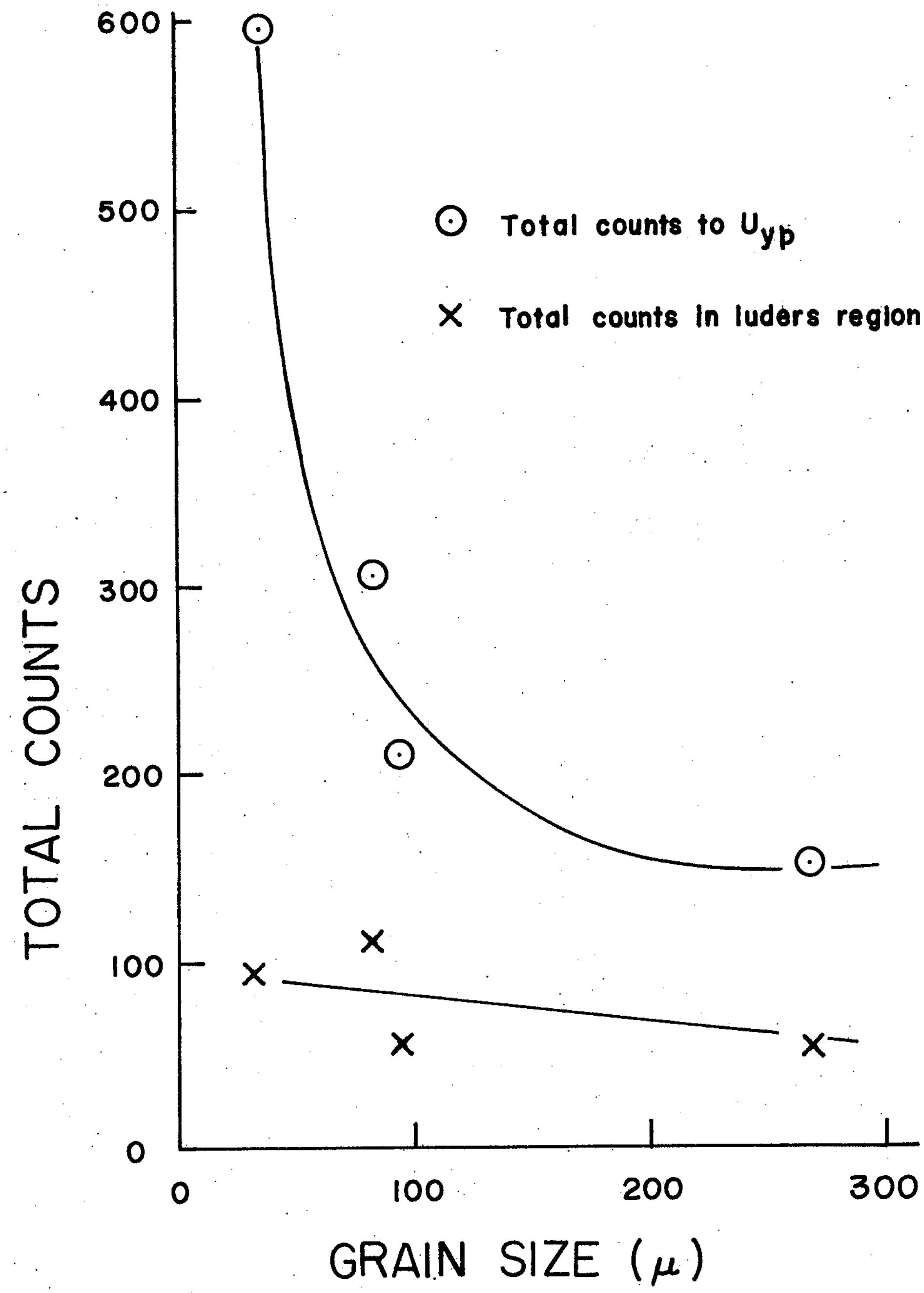

Figure 24: Total Counts up to the Upper Yield Point and during the Luders Region vs. Grain Size for Sample Set 1. Trigger Level 79.4μv.

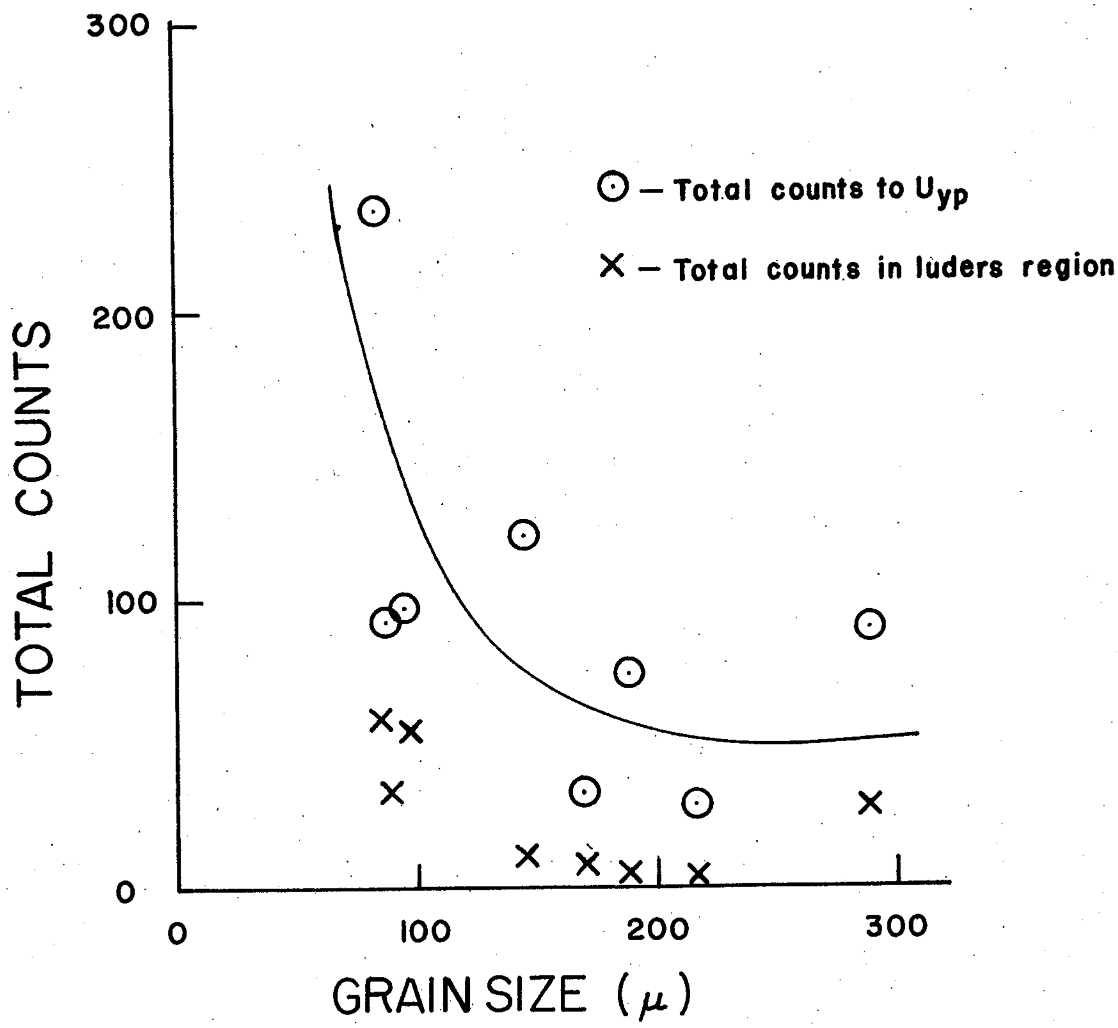

Figure 25: Total Counts during Microstrain and Luders Region vs. Grain Size for Sample Set 2. Trigger Level =158μv.

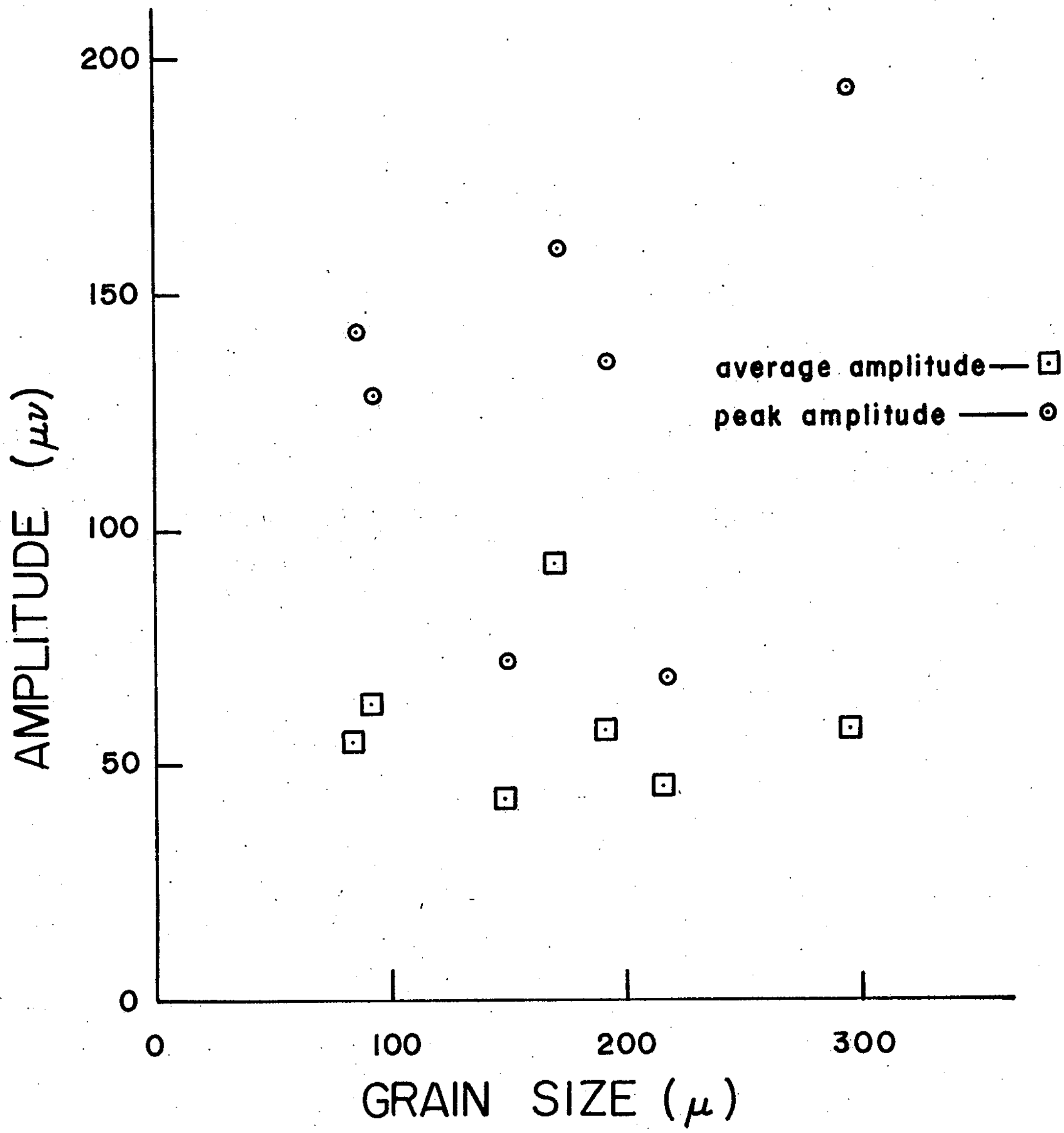

Figure 26: Average and Peak Amplitude to σ_{1y} vs. Grian Size.

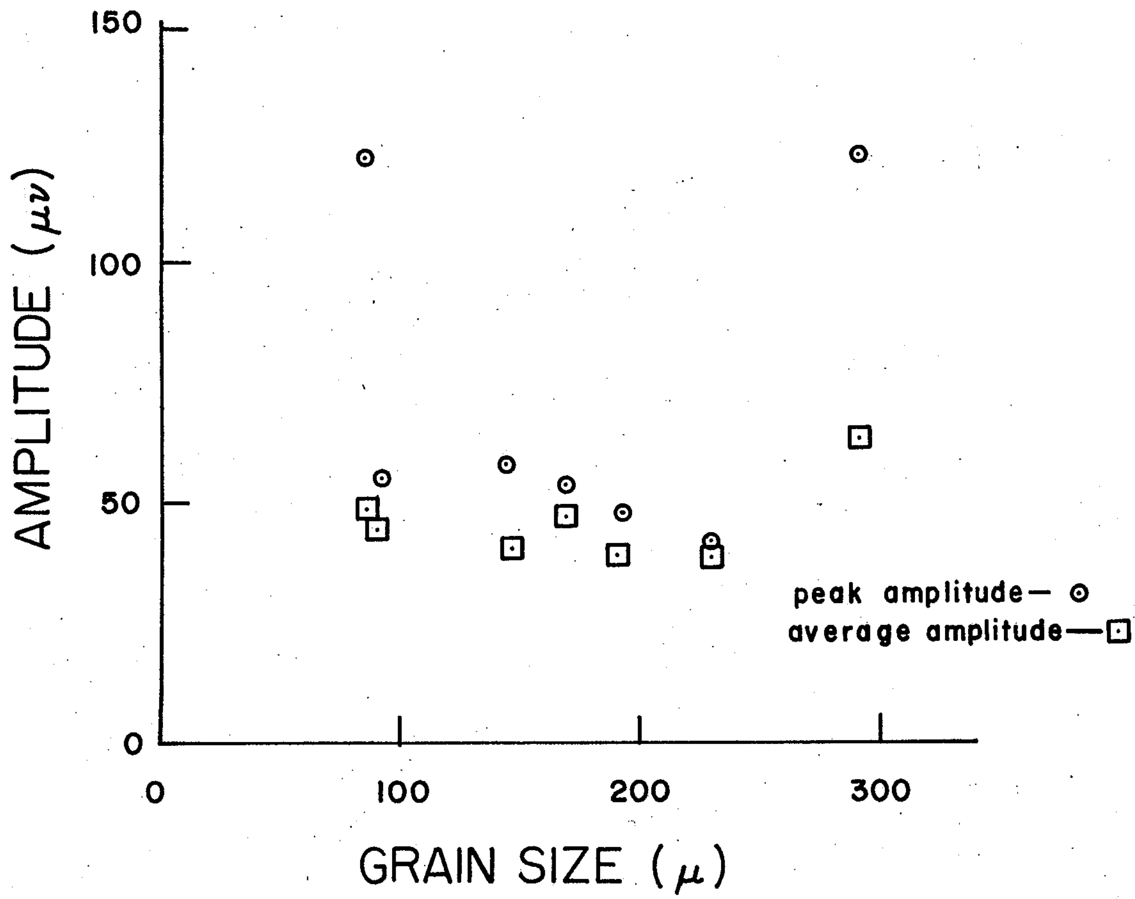

Figure 27: Average and Peak Amplitude from the Upper Yield Point to 2.5% Strain vs. Grain Size.

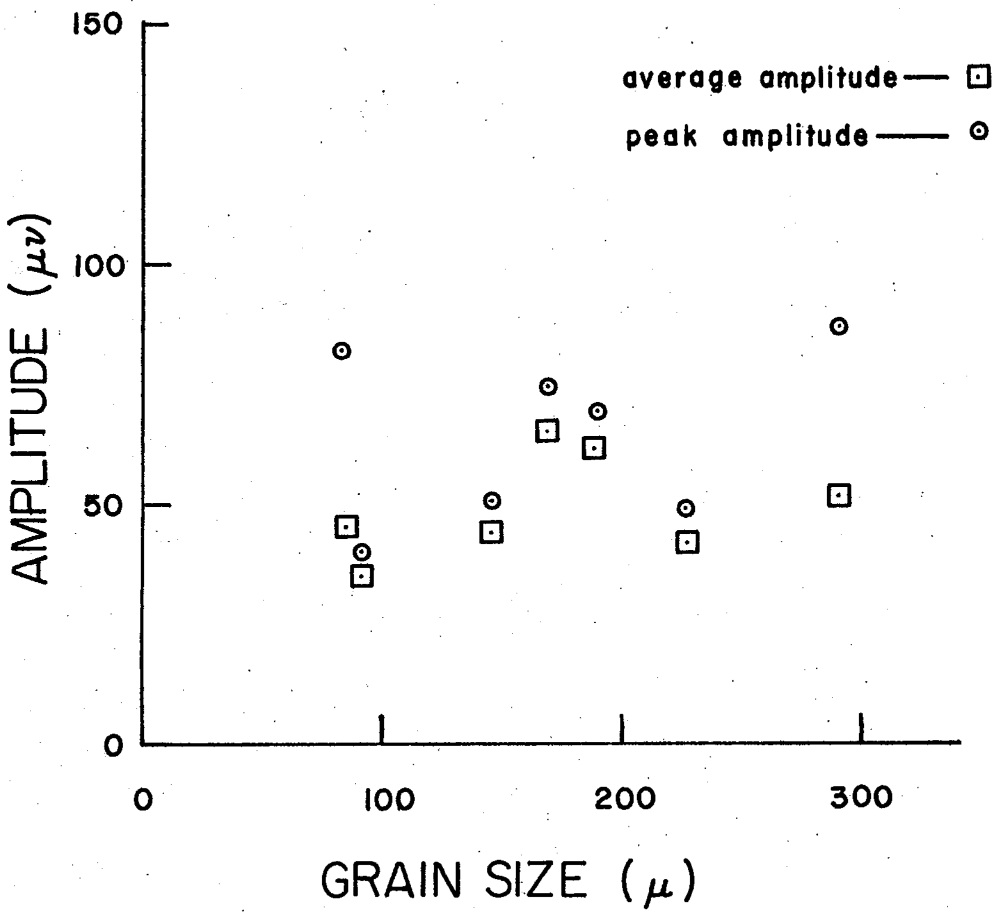

Figure 28: Average and Peak Amplitude from 2.5% to 5.0% Strain vs. Grain Size.

Figure 29 shows the stress levels at which signals were photographed and Figures 30 through 40 show some of these pulses.

These were in general two catagories of emissions. Type 1 (shown in Figure 37) appeared to be a form of ring down pulse, but was made up of either many frequency components or the sum of two or more emissions which occurred at the same time. Type 1 pulses always decayed rapidly after the peak amplitude was reached. The second type of emission, Type 2 (Figure 30) appeared to be a combination of many emissions of varying amplitude occurring one after another over a period of time. Due to the nonuniformity of pulse shapes, it was often a subjective judgment whether any particular emission was labelled a type 1 or type 2 pulse.

An attempt was made to analyse the emissions with respect to their fundamental frequency. The procedure was to count the number of wavelengths in a certain time interval and calculate the frequency. This was rather a rough calculation since harmonics, interference, and noise can affect the signal. Fundamental frequencies calculated in this way ranged from 136 khz to 658 khz. Type 1 pulses appeared to have frequencies in the range from 200 to 250 khz in the fine grain size and from 136 to 455 khz in the coarse grain sized samples. Type 2 emissions had frequencies ranging from 166 to 659 khz. In general, there appeared to be no grain size dependence of either frequency or pulse type. However, more sophisticated methods of analysis are required to substantiate this observation.

Figure 40 shows two pulses captured .25 msec apart. These pulses are typical of transient noise which was introduced into the system from outside sources from time to time. These pulses are easily recognized since they often had a spike like appearance on the oscilloscope AE monitor and occurred even when no specimens were being pulled.

Note that comparisons between Figures 29 and Figures 30 to 40 can be made with the use of Table 6 which lists the Pulse number, type, peak amplitude and frequency for each grain size.

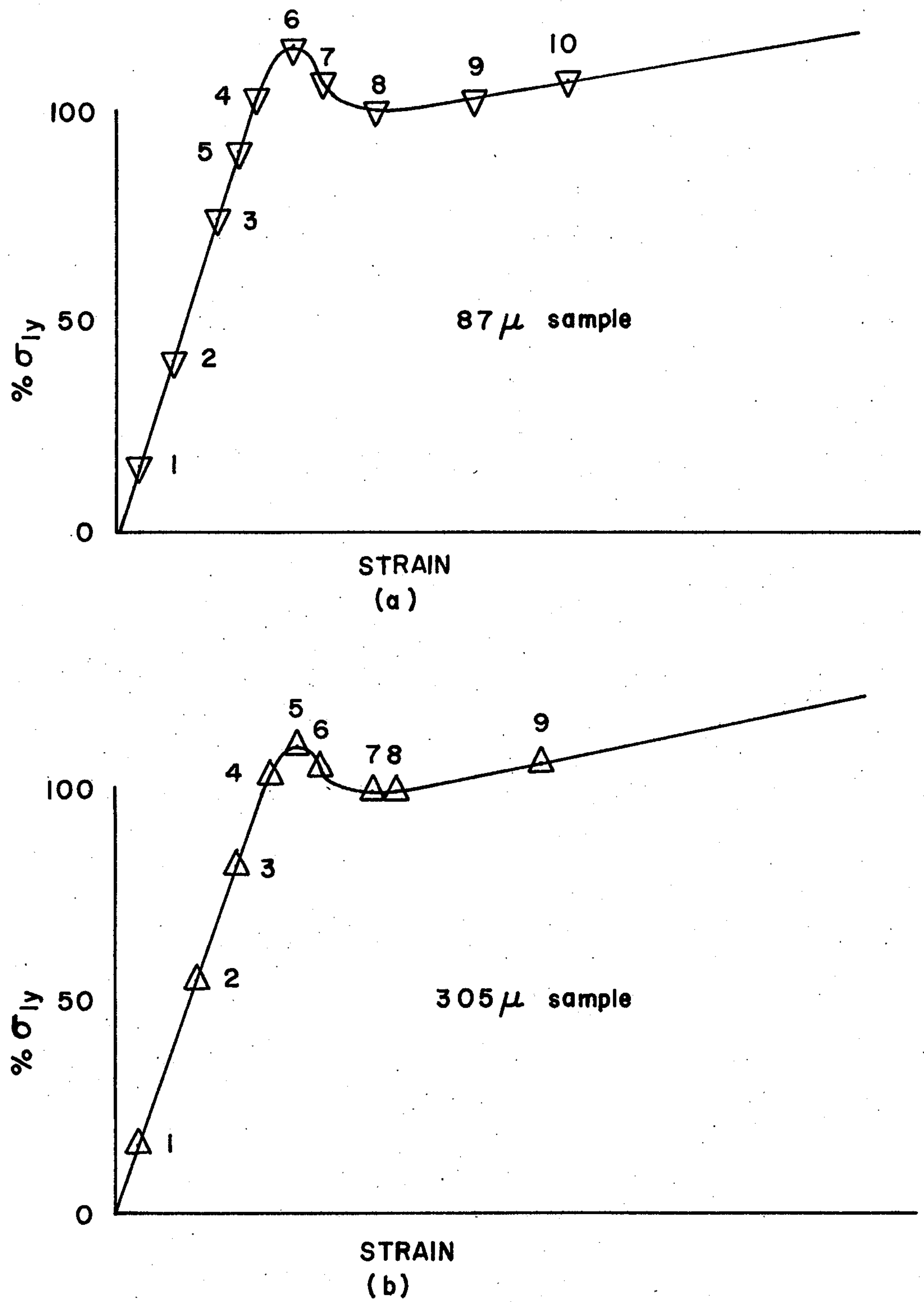

Figure 29: Positions at which Acoustic Emission Pulses were Photographed.

outside sources from time to time. These pulses are easily recognized since they often had a spike like appearance on the oscilloscope AE monitor and occurred even when no specimens were being pulled.

Note that comparisons between Figures 29 and Figures 30 to 40 can be made with the use of Table 6 which lists the Pulse number, type, peak amplitude and frequency for each grain size.

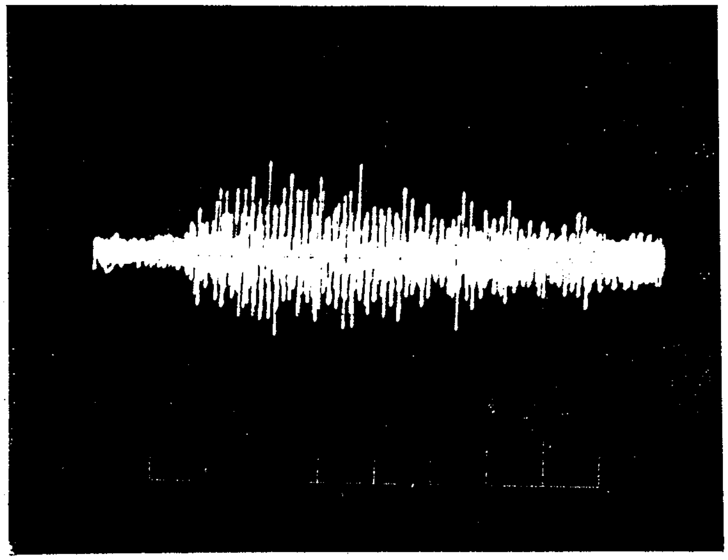

Figure 30: Pulse 3 from 87µ Specimen. Abscissa =.102 ms/div.

Ordinate = 1v/div.

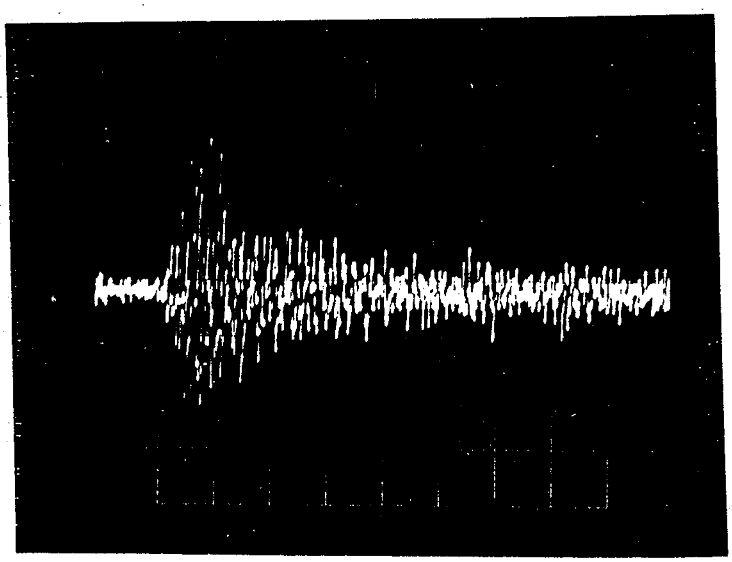

F Figure 31: Pulse 5 from 87µ Specimen. Absissa =.05 ms/div.

Ordinate = 1 v/div.

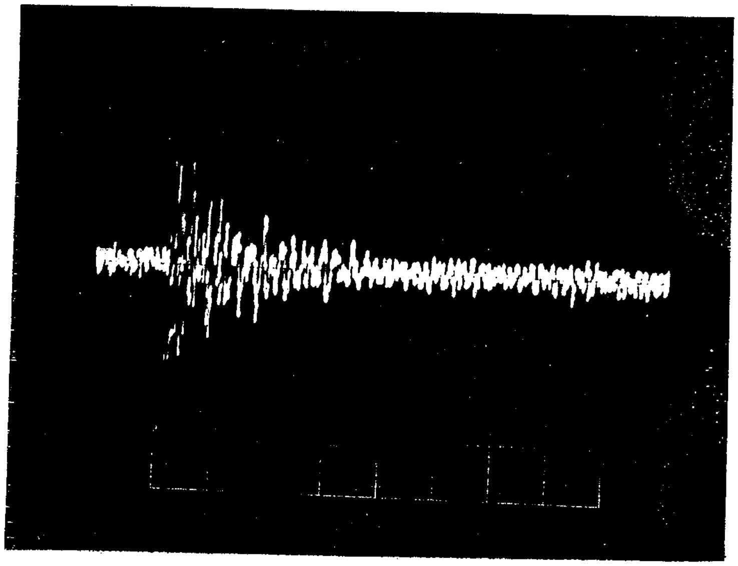

Figure 32: Pulse 6 from 87μ Specimen. Abscissa =.05 ms/div.
Ordinate = 1 v/div.

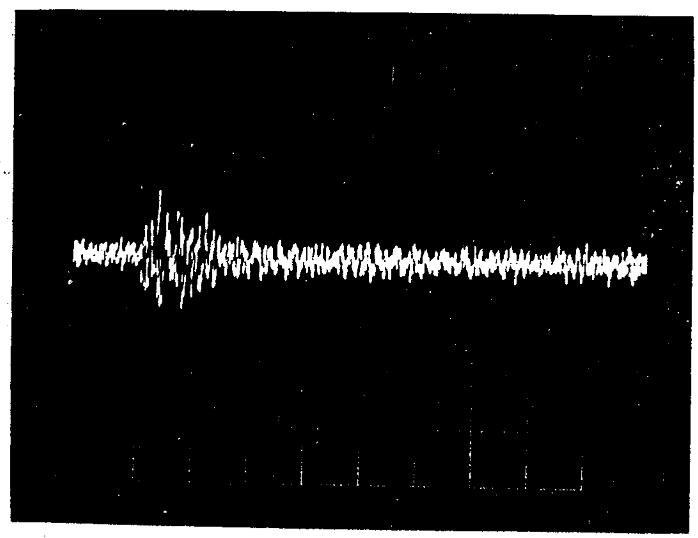

Figure 33: Pulse 8 from 87μ Specimen. Abscissa =.05 ms/div.
Ordinate = 1 v/div.

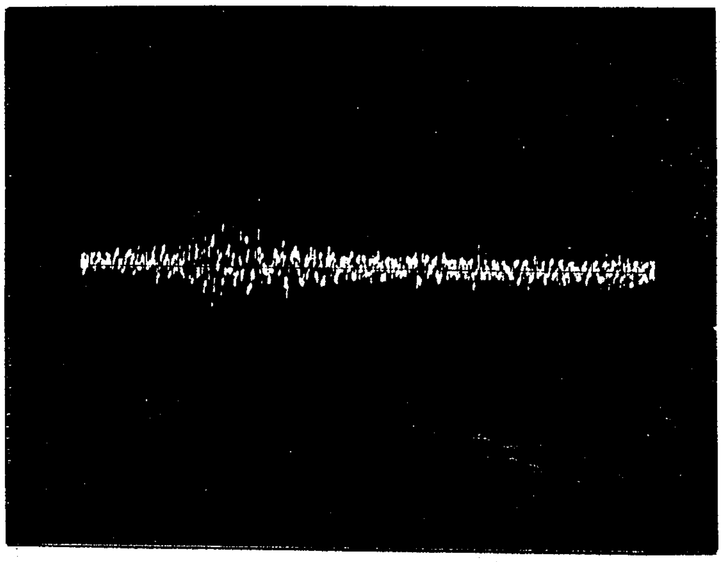

Figure 34: Pulse 9 from 87μ Specimen. Abscissa =.05 ms/div.

Ordinate = 1 v/div.

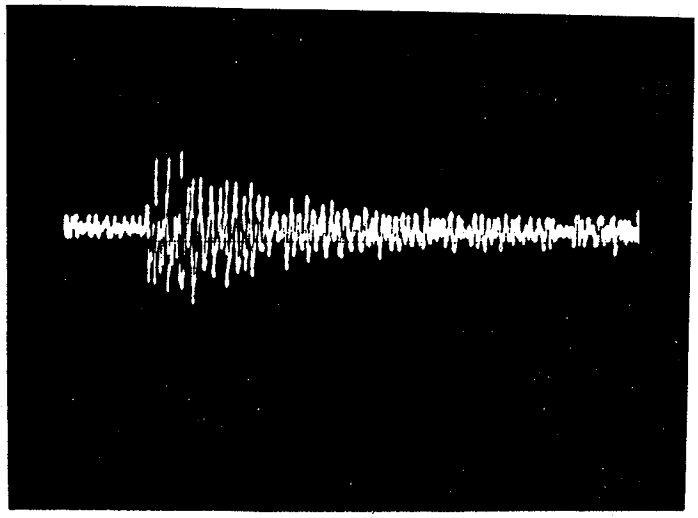

Figure 35: Pulse 3 from 305μ Specimen. Abscissa =.05 ms/div.
Ordinate = 1 v/div.

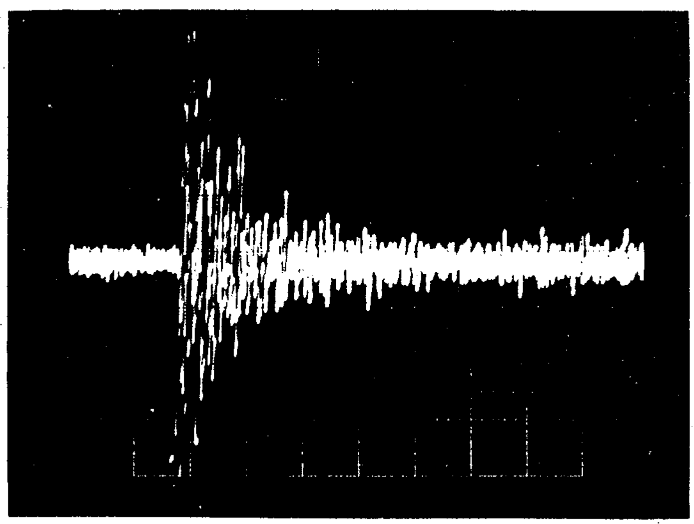

Figure 36: Pulse 4 from 305μ Specimen. Abscissa =.10 ms/div.
Ordinate = 1 v/div.

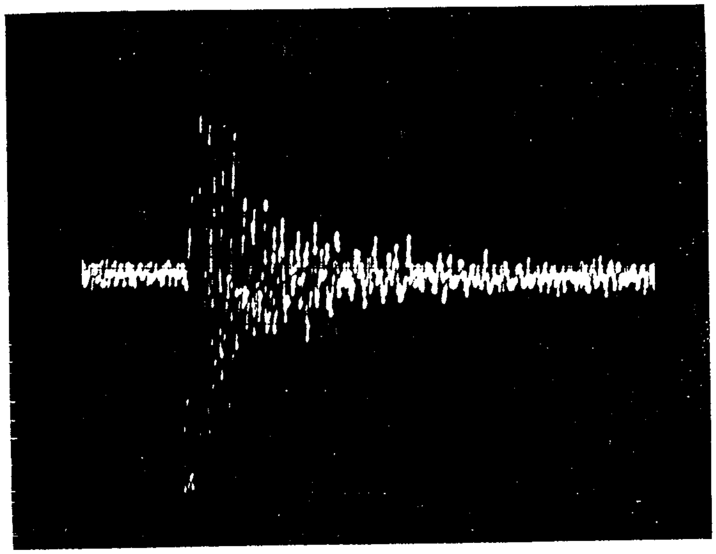

Figure 37: Pulse 5 from 305μ Specimen. Abscissa =.05 ms/div.
Ordinate = 1 v/div.

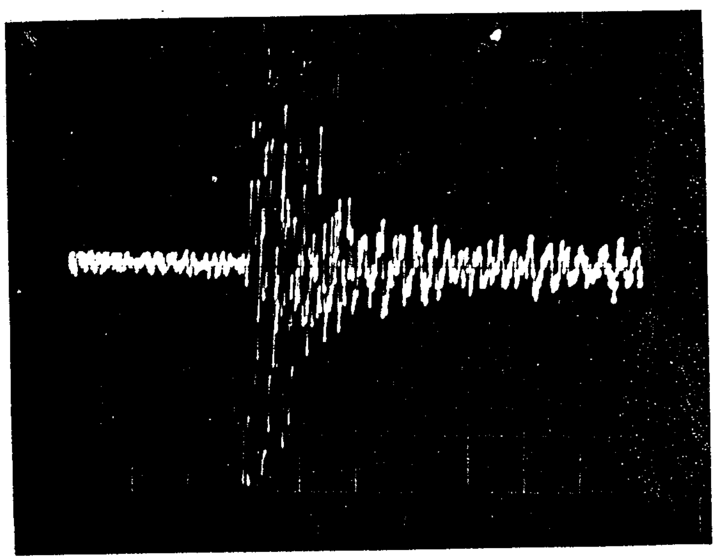

Figure 38: Pulse 7 from 305μ Specimen. Abscissa =.05 ms/div.
Ordinate = 1 v/div.

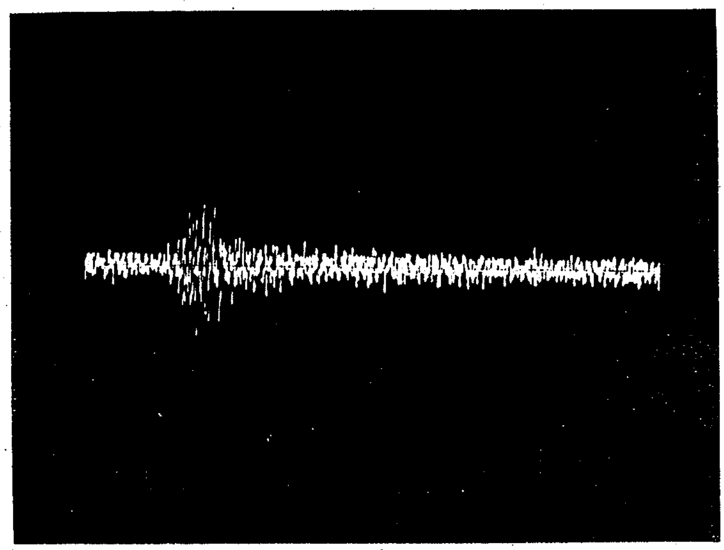

Figure 39: Pulse 10 from 305μ Specimen. Abscissa =.05 ms/div.
Ordinate = 1 v/div.

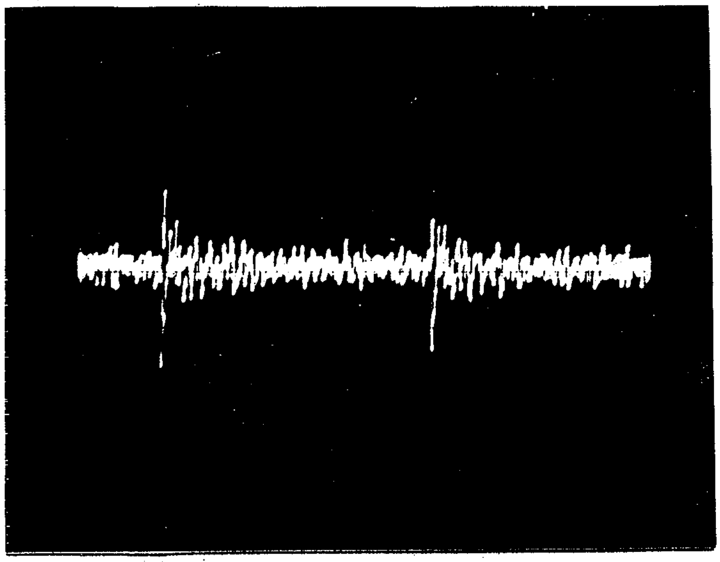

Figure 40: Pulse 8 from 305μ Specimen. Abscissa = .05 ms/div.
Ordinate = .1 v/div.

87 μ					305 μ				
Pulse No.	Type	% Yield (Lower)	Peak Amp (V)	Freq. Khz	Pulse No.	Type	% Yield (Lower)	Peak Amp (V)	Freq. Khz
1	2	16	1	659					
					1	2	17.2	2	455
2	1	42	4	244					
					2	2	56.7	1.6	156
3	2	75	1.8	185					
					3	1	83	1.5	234
5	1	90	3	224					
4	2	105	2	586	4	1	105	4	455
6	1	116 U_{yp}	3.2	225	5	1	110 U_{yp}	4	136
7	1	108 ydr.	1.2	215	6	2	ydr.	1.6	293
8	2	L_{yp}	1.2	166	7	1	L_{yp}	4	195
10	2	whr	1.3	296	8	Trans-ient			

TABLE 6

PULSE ANALYSIS

5.0 Discussion

The results and their implications on the yield and plastic flow phenomena in Nb will be discussed in subsections termed the microyield and macroyield regions. Discussion of the microyield region includes:

1. Mechanisms of slip initiation
   - (a) A description of the grain boundary ledge theory of dislocation multiplication.
   - (b) A description of possible dislocation sources in Nb which result in a homogeneous distribution of dislocations.
2. A discussion of slip band formation; slip band sources and their grain size dependence.
3. A discussion of the grain size dependence of the microyield stress (σ_{my}).
4. The implications of the acoustic emission results with respect to dislocation processes in the microyield region.

The macroyield region is discussed in the subsections entitled.

1. Lüders Band Nucleation and Propagation.
2. The Work Hardening Region.

Finally a short section on the analysis of individual acoustic emission events is presented.

5.1 Slip Initiations

Previous work on Fe-Si, MgO and Nb indicate that σ_i is relatively independent of grain size. The present results on Nb are in agreement with the previous work as can be seen in Figure 17. However, at σ_i, slip bands as well as a small increase in general dislocation density were observed in coarse grain sizes (Figure 10) whereas finer grain sizes showed only a uniform increase in dislocation density with no apparent slip line activity. Why this maybe so is discussed in the following two subsections.

5.1.1 Grain Boundary Ledge Theory of Dislocation Multiplication

It is apparent from this work and others on Nb (1), (4), (6) that in coarse grain sizes slip can be initiated at or near the grain boundaries and is observed as a row or band of etch pits extending into the grain interior. This implies that a grain boundary source mechanism is responsible for slip line initiation.

Tangri and Tandon (30) described a way by which dislocations may be created by homogeneous nucleation at stress concentration points in a grain boundary. According to their model the grain boundaries consist of ledges of various dimensions and each ledge can be assigned a stress concentration factor, K_G, which is a function of ledge size, the angle the ledge is to the grain boundary (flank angle) and the radius of curvature of the boundary during the transition from the grain boundary to the ledge. Usually the larger the ledge size the higher the stress concentration factor. Another stress concentration factor comes into play if one takes into account the elastic incompatibility between two grains. This factor, K_E, has been approximated by Tangri and Tandon (30) to be 2. The product of K_G and K_E approximates the total stress concentration factor in the vicinity of a ledge.

As the applied stress, σ_a is increased, the largest ledge will first achieve a concentrated stress of $\mu/25$, enough to nucleate dislocations in an area very close to the ledge. As σ_a is further increased, smaller ledges will also achieve the stress level necessary for grain boundary source activation. If it is assumed that σ_i is the minimum required applied stress necessary for the above mechanism to operate, and the shear modulus of Nb is known then the stress concentration factor, K, needed for slip initiation can be found.

$$\mu \text{ for Nb} = 3.82 \times 10^3 \text{ kg/mm}^2$$

$$\sigma_i = 3 \text{ kg/mm}^2$$

$$\therefore K = \frac{\mu}{(25)\ \sigma_i} = \frac{3.82 \times 10^3}{25(3)}$$

$$K = 50$$

But $K = K_G(K_E)$ and $K_E = 2$

$$\therefore K_G = 25$$

Therefore a ledge which has a stress concentration factor of 25 is the first to be activated on straining. Tangri et al's (30) results indicate that this value of Kg corresponds to a ledge size of 300 to 600 A^o with a flank angle of 90^o. This is a reasonable size to expect and the calculation lends support to the ledge theory of homogeneous nucleation of dislocations in coarse grain size Nb.

However, the use of σ_i as an approximation to the stress needed for source activation is questionable since at σ_i slip bands already appeared in coarse grain sizes indicating that the stress necessary for the activation of a source has been exceeded. The physical meaning of σ_i must be studied in greater detail.

The lowest stress at which dislocation multiplication was first observed by the etch pit technique has been defined as σ_i. There are two conditions which dictate at what stress σ_i will occur. These are:

(a) σ_i must be above the stress required for dislocation sources to operate. This condition is inherent in the definition of σ_i.

(b) σ_i must be above the friction stress of the material. Let it be assumed for a moment that a source has nucleated a dislocation. If the friction stress (σ_f) is greater than the applied stress (σ_a), a freshly nucleated dislocation cannot escape from the immediate vicinity of its source. If the source is a grain boundary ledge or another dislocation, the distance between the new dislocation segment and the source will not be great enough for their etch pits to be resolved under a microscope, hence σ_i has not occurred. If σ_a is greater than σ_f the fresh dislocation can glide across the grain, and upon etch pitting be resolved. Ideally, if condition (a) has been met then a step loading experiment using very fine increments of stress would give a very accurate determination of σ_i and would also give σ_f i.e., $\sigma_i = \sigma_f$. In the present work slip at stresses below 3 kg/mm^2 ($\sim$ 40% σ_{ly}) was not investigated because of a very real danger that the specimens would be damaged due to etch pitting and preparation procedures. Since σ_i had occurred at 3 kg/mm^2 (Figure 17) it is safe only to assume that the friction stress and source activation stress has been overcome.

Therefore in the calculation of K_G the use of σ_i as the applied stress necessary for source activation is an overestimate of the true value and will result in an underestimate of K_G and ledge size. However, even if the minimum stress for source activation is one third that of σ_i (i.e., 1 kg/mm^2 or $\sim$ 10% of σ_{ly}) the ledge size will be approximately 1500 A^o which is not unreasonable in a large grain size.

It is concluded that in coarse grained Nb, when σ_a is greater than σ_f, and a grain boundary ledge source has been activated, a row of dislocations will be produced and slip is initiated.

5.1.2 Sources Giving a Homogeneous Distribution of Dislocations

The experimental results shown in Figure 18 and Table 4 indicate that slip initiation in fine grain sizes results in an increase in dislocation density that is homogeneous throughout the sample. This increase also occurs in coarse grain sizes at least up to the stress where slip lines appear via etch pits.

There are two models which may explain this phenomena.

The first is the grain boundary dislocation generation model proposed by Li (15). A grain boundary ledge in this model is considered as an absorbed edge dislocation such that under the influence of an external applied shear stress, the ledge is removed from the boundary generating a dislocation in the grain interior. This type of source can not produce more than one dislocation per source. Therefore, if many such sources are located randomly on the grain boundary surface, and some are orientated such that slip can occur, then fresh dislocations will appear throughout the grain in a random pattern.

The second model involves the generation of dislocations inside the grain. Dislocation multiplication is defined as any mechanism which increases the length of dislocation line. This may be achieved for example, by the bowing of a dislocation or cross slip. Both these mechanisms require the presence of dislocations in the interior of the grain. This requirement is fulfilled by the creation of grown in dislocations during the annealing process. Grown in dislocations are not usually located in a slip plane and therefore cannot move as a whole. However, portions of a grown in dislocation may be suitably orientated for slip on a slip plane. If the applied stress is greater than the friction stress, these portions may bow out and multiplication will have taken place. If the bowed segment in a dislocation line intersects the surface of the sample then two new etch pits will be observed and thus the etch pit density has increased. Since grown in dislocation lines are nearly randomly located in a grain, then the new dislocation etch pits will also be randomly distributed.

Figure 6 shows that the grown in dislocation density (ρ_0) increases with decreasing grain size. Therefore, from the above analysis one would expect that the random dislocation density would increase at a faster rate with stress in fine grain sizes than in the coarse due to the increased number of potential sources. Figure 18 shows this to be true, however, coarser grain sizes are being deformed by slip lines and bands and these are discussed in the next section.

5.2 Sources of Slip Bands in Nb

In Nb slip band sources are thought to be near the grain boundaries (1), (4), (6). Therefore the grain size dependence of the applied stress at which slip lines or bands were first observed (σ_{Sl} in Figure 17) may be the result of difference in grain boundary source structure between fine and coarse grained Nb. If we assume as did Tandon and Tangri that grain boundary ledge size, in general, increases with increasing grain diameter, then the higher stress concentrations of the ledges in the coarse grain size will nucleate dislocations at lower applied stresses than the smaller ledges of the fine grain size.

The operation of these ledge sources creates slip lines which subsequently become slip bands. Many authors use the terms "slip lines" and "slip bands" synonymously, therefore, it is felt that some clarification of these terms is needed.

A slip band refers to a band of etch pits, of variable width which may be formed in one of two ways:

1. At a certain stress a regenerative source produces a slip line, that is, many dislocations on the same slip plane

with the same burgers vector. If many of these sources operate on parallel closely packed slip planes a slip band will result. This slip band then consists of many closely packed slip lines, each line separate from the others with little interaction with neighbouring slip lines. The slip bands in Fe-Si (5) and MgO (31) appear to be the result of the process described above, at least in the early stages of deformation.

2. At a certain stress a regenerative source produces a slip line. A pile up is formed when the slip line encounters a grain boundary or other obstacle. The dislocations in the slip line are able to cross slip if the material has a high stacking fault energy and many available slip systems (unlike Fe-Si and MgO). Any dislocation in the pile up will cross slip if it has a pure screw component that intersects another slip plane which is under a shear stress favorable for slip. The dislocation, after moving a few burgers vectors, can cross slip back to a plane parallel to its original since the resolved shear stress is greater on that set of planes. This process is commonly referred to as double cross slip. Therefore, by repetitive double cross slip a slip band is formed. In Figure 10 a few slip lines and slip bands can be seen. The slip bands do not appear to be made up of rows of slip lines as in MgO and Fe-Si but appear to be made up of many dislocations

on many different slip planes. There is often a change in the width and dislocation density of the bands from one end to the other. These factors indicate that cross slip is taking place on a massive scale within the bands.

Slip line and band propagation through grain boundaries in the microyield region appeared to be easy, often being observed at the same time as the first slip bands were observed (Figure 10 and 11). In Evans (1) as well as this work, it was frequently noted that etch pits in adjacent grains were similar in shape and orientation suggesting that the grains were closely orientated. The fact that slip lines and bands often show little change in direction after crossing from one grain to another proves the fact that slip planes on either side of a grain boundary are often closely orientated.

Figures 12 and 13 show that at about 80% of σ_{ly}, cross slip is obvious in all grain sizes. Above 80% of σ_{ly} to the upper yield point, fully yielded grains become evident (i.e., grains with dislocation densities so high that resolution of the individual etch pits by optical microscopy becomes impossible), however, before this becomes the rule rather than the exception upper yield occurs.

5.3 The Microyield Stress (σ_{my})

As shown in Figure 17 σ_{my}, increases with a decrease in grain size. This may be the result of the characteristics of grain boundary ledge dislocation generation and grain diameter.

In coarse grain sizes ledges produce dislocations and these may slip a distance approximately equal to the grain diameter, cross slip also occurs and hence much deformation takes place at low stresses.

In fine grain sizes ledges do not produce pile ups of dislocations until higher stresses than in the coarse grained samples and the slip distance is smaller for any individual dislocation. Owing to the decreased slip distance available per dislocation, a fine grain size requires a higher density of dislocations and therefore a larger number of activated sources than a coarse grain size to achieve microyield (stress at 6.25 x 10^{-6} strain).

Hence, the increase of σ_{my} with a decrease in grain size is due to a smaller ledge size and a shorter average slip distance per dislocation.

5.4 Acoustic Emission Implication in the Microyield Region

Acoustic emission was observed to occur almost at the onset of straining. As shown in Figure 26, AE amplitude showed no discernable variation with grain size up to the upper yield stress. This observation implies that AE occurs from the same types of sources in both fine and coarse grain sizes. Etch pitting has shown that there are two main sources of dislocations in the microyield region. Homogeneous nucleations of dislocations from grain boundary ledges should give the same AE amplitude in all grain sizes and hence, no variation between grain size and AE from this source is expected. Likewise, cross slip should give little or no AE variation with grain size, however, AE signals from a cross slip mechanism should be very low in amplitude (29) and may indeed be below the equipment noise level.

Therefore, it is suspected that grain boundary source operation is responsible for the AE results in the microyield region.

Figures 24 and 25 show that the total AE counts up to the upper yield point increase with decreasing grain size. As shown in the sub-section dealing with the microyield stress, smaller grain sizes require a higher density of activated grain boundary ledge sources than the coarse grain sizes because they require a larger dislocation density for any particular strain. If it is assumed that all the dislocations produced in the microyield region were due to grain boundary ledge sources, then AE total counts would be expected to increase as grain size became smaller. Although cross slip does occur in this region it is not expected to influence the trend of the observations.

Tandon and Tangri's (18) experiments on Fe-Si show the opposite trend in that AE total counts up to .9 σ_{ly} increase with grain size. In explaining their results they assumed that larger grain sizes had larger ledge sizes and hence at any particular stress a larger number of sources are activated. Furthermore, with progressive increase in stress, source activation near ledges would increase at a faster rate in coarse grain as compared to a fine grain sample. The main objection to both the present results and Tandon and Tangri's (18) is that no study of ledge density or size as a function of grain size has been undertaken. It is suggested that a study of this type be performed in the future.

5.5 Macroyield

5.5.1 Lüders Band Nucleation and Propagation

Each specimen, upon reaching the upper yield point, exhibited two or more areas of highly deformed grains. These areas were located near the shoulders of the sample and also, as was the case in about 50% of the samples, in the gauge length. It is reasonable to assume that the higher stress concentrations resulting from the curvature of the sample shoulder were responsible for the yielded regions in that area. Also, areas within the gauge length may have been yielded by particularly severe stress concentrations. The Lüders band is born during the yield drop and it propagates along the length of the specimen in the direction of the tensile axis. In this process the Lüders band front, J-J in Figure 16, moves with constant velocity from grain to grain to the left. Grains in the region I-I of Figure 16 are in the area where intense slip activity is about to start, as the result of the Lüders band. As we move toward the Lüders band front from I-I dislocation densities increase, apparently by an increase in slip band or line density and by slip band broadening as a result of cross slip.

One extremely important and revealing observation made in the macro-yield region is the AE counts and amplitude decrease immediately after the upper yield point, and stay at a low value until after the work hardening region occurs. Typical results are shown in Figure 22 and 23. It is noted that this change in AE activity occurs at the same time as Lüders band nucleation and propagation. While in Fe-Si this gives rise to large increases in the nucleation of dislocations at grain boundaries resulting in a grain size dependence of σ_{ly} and a large increase in AE activity, it is felt that in Nb this source of dislocations nearly ceases to operate and that other multiplication mechanisms become dominant which result in a σ_{ly} which is not dependent on grain size (Figure 17), and a decrease in AE activity and amplitude. Cross slip is the most likely mechanism since slip bands appear to broaden as the Lüders band front approaches. Pile up break away is thought to be a major source of slip between grains and a source of AE. Due to the large number of slip systems in Nb it is likely that there is only a little misorientation between two slip planes in two adjacent grains. This is supported by the fact that slip lines were often seen to pass through a grain boundary with little or no apparent change in direction. Therefore, a slip line or band would see little or no resistance from a grain boundary and slip through it would be an easy process. Therefore, AE would be minimal approaching that of dislocations in free glide.

Further support that Lüders band propagation in Nb is not the result of the operation of grain boundary sources comes from the load cycling experiments. In these tests the same trends were observed as those in experiments by Koppenaal and Evans (4). The load was cycled until the microyield stress was obtained, on subsequent cycling the minimum stress, under the experimental limitations, required for further plastic deformation decreased as shown in Figure 19 by the dashed line. σ_{FL} represents the minimum stress required for plastic deformation after a prestrain. Table 5 shows that σ_{FL} does not vary appreciably with grain size, and Figures 19 and 20 show that it remains relatively constant over several stress cycles. It is proposed that σ_{FL} is the minimum stress required for multiplication of dislocations if mobile dislocations are present in the grains, and in fact represents the minimum stress necessary to propagate a Lüders band. If σ_{FL} was dependent on a grain boundary source mechanism then one would expect a grain size dependence like that observed for σ_{my}, however, as noted, no such relationship exists. It is evident therefore that at σ_{FL} sufficient mobile dislocations exist in the material for the propagation of yield and that this must take place via cross slip by some other grain size independent mechanism.

Therefore, it is proposed that Lüders band propagation and the grain size independence of the lower yield stress is the result of massive cross slip and interaction of dislocations produced by sources in the microyield region.

A comment on the general shape of the curves in Figure 19 and 20 is in order.

After the microyield stress was obtained and the specimen unloaded to D, the load was reversed and the stress in the sample began to rise. At point "F" an increase in plastic strain was resolved by the strain gauge apparatus. Therefore, at stresses lower than F, dislocation activity must be present in the sample to produce the observed strain. On loading beyond "F" this activity increases and is portrayed by the decreasing slope of the line F-E. At "E" the load was reversed, however, straining in the sample was still noted. This may be attributed to the fact that the applied stress is still,of course, higher than the friction stress and that any mobile dislocations created during the loading portion of the curve may move or interact with others, thus straining the sample.

Plastic strain continues as the load is decreased until at least that load where the plastic straining is so small that it becomes undetected by the strain gauge apparatus, and this is demarked by the point where the load and unloading curves cross. This point could therefore be described as the elastic limit of the specimen after a certain known prestrain, and certainly describes the minimum stress at which further observable plastic deformation will take place.

5.5.2 Work Hardening Region

Once the Lüders band has covered the entire gauge length of the whole specimen, the sample enters the work hardening region. All grains have undergone extensive slip in the Lüders region and each grain has a high dislocation density. Basic dislocation processes occurring during the work hardening region are: dislocations on two different slip systems running into each other, jog formation, dislocation pile up at barriers and their break away, formation of multipoles and their rearrangement and finally wall and cell formation. Only pile up break away and the rearrangement of multipoles are expected to give rise to AE pulses (27). Figures 22 and 23 show that some AE activity does occur in the work hardening region and that the smaller grain size has more AE activity than the large grain size. This is probably due to the finer substructure of the small grain size and the reduced free flight distance of the dislocations. Thus the frequency of break aways and the resulting AE is expected to increase with a decrease in grain size.

5.6 AE Pulse Analysis

The present AE pulse analysis gave little in terms of data suitable for explaining the yielding phenomena. However, a few points are noteworthy and may be of some significance to future investigations.

As noted there appeared to be two general types of pulses. Type 1 is characterized by the maximum amplitude being located close to the beginning of the pulse and by a rapid decay of the signal to the noise level (Figure 36). Table 6 shows that 5 out of the 8 type 1 pulses recorded had a fundamental frequency of 200 to 250 khz. Owing to the similarities between type 1 pulses it is felt that these may be the result of the operation of a single source with many frequency components, or the operation of two or more sources of the same kind at the same instant with a resulting signal interference. Pulse type 2, as shown in Figure 30, was characterized by a seemingly random signal above the noise level. Their fundamental frequencies ranged from 156 to 659 khz. Because of their wide frequency range type 2 pulses may be the result of sources being triggered by one another over a short period of time, or by sources which emit dislocations at an extremely fast rate.

Figure 40 shows two identical pulses. These pulses were the typical result of random disturbances from outside sources on the AE system, and occurred randomly throughout all the tests. Because of this randomness it is felt that the experimental results and the conclusions drawn from them are not seriously affected.

6.0 Conclusions

1. It has been shown by etch pit techniques that dislocations in Nb are initially produced at a stress level significantly lower than that of the microyield stress and that these dislocations are nucleated by two different types of sources. Grain boundary ledge sources result in slip lines in coarse grained material, and, sources within the grains (probably grown in dislocations) result in a homogeneous distribution of new dislocations in both coarse and fine grained material.
2. The stress required for slip line initiation decreases with increasing grain size. If grain boundary ledge size increases with grain size, the subsequent increase in the stress concentration at the ledges will nucleate dislocations at lower stresses in the coarse grain sizes than in the fine. Activation of these sources results in slip lines. Cross slip is responsible for the broadening of slip lines into slip bands.
3. The microyield stress (corresponding to a plastic strain of 6×10^{-6}) shows a Hall Petch relationship in terms of grain size. The grain size dependence is attributed to the change in dislocation density with grain size. The dislocation density is higher in finer grain sizes due to a shorter slip distance, also grain boundary ledge source activation requires higher stresses in finer grain sizes; these two combined explain the observations. This hypothesis is supported by the fact that acoustic emission results indicate that there is more dislocation source activity in fine grain sizes than the coarse since the total counts up to the upper yield point increase with decreasing grain size.

4. Lüders band propagation is mainly the result of cross slip and easy slip between grains, this is reflected in the AE results by a substantial decrease in amplitude of the emissions after the upper yield point is reached. The end result is that little or no grain size dependence of σ_{ly} is observed.
5. Dislocation process in the work hardening region are not grain size dependent. Smaller grain size samples have higher rates of AE. This is ascribed to the development of finer substructures and smaller free flight distances for dislocations in fine grained samples.

REFERENCES

1. Evans, P.R.V., J. Less. Common Metals, 6 (1964), 253-265.
2. Vardiman, R.G. and Achter, M.R., Trans. of Met. Soc. of AIME, Vol. 242, February 1968, p. 196-205.
3. Van Torne, L.J. and Thomas, G., UCRL Report No. 10515, (Berkeley), November 1962.
4. Koppenaal, T. and Evans, P.R.V., J. Inst. of Met., Vol. 92, 1963-64, p. 238-241.
5. Suits, J.C. and Chalmers, B., ACTA Met., Vol. 9, September 1961, 854-860.
6. Brentnall, W.D. and Rostoker, W., ACTA Met., Vol. 13, March 1965, p. 187-198.
7. Braun, N. and Ekwall, R.A., ACTA Met., Vol. 110, November 1962, p. 1101-1107.
8. Low Jr., J.R. and Guard, R.W., ACTA Met., Vol. 7, March 195 , p. 171-179.
9. Conrad, H., J. of Iron and Steel Inst., August 1961, p. 364-375.
10. Hirsch, P.B., Appendix to Thomas and Nutting, J. Inst. of Metals, 86, 13 (1957).
11. Cottrell, A.H., Trans. TMS-AIME, 1958, v. 212, p. 192.
12. Conrad, H., Feuerstein, S. and Rice, L., Mats. Sci. and Eng., 2, (1967), 157-168.
13. Conrad, H. and Hays, W., Trans. Am. Soc. Metals, 56, (1963), 249.
14. Conrad, H., N.P.L. Symp. HMSO (1963), p. 475.
15. Li, J.C.M., Trans. of M.S.-AIME, v. 227, (1963), 239-247.

16. Li, J.C.M. and Chau, Y.T., Met. Trans., V. 1, (1970), 1145-1159.

17. Tangri, K., Lloyd, D. and Malis, T., (1972) Proc. Int. Symp. "Fifty Years of Metallurgy", held at Banaras, India (December 1972).

18. Tandon, K. and Tangri, K., Mats. Sci. and Eng., 20 (1975), 47-54.

19. Westbrook, J., Fliesher, Schodler and Johnson AIME paper presented at New York (1964).

20. Adams, M.A., Roberts, A.C. and Smallman, R.E., ACTA Met., 8 (1960), 328.

21. Johnson, A.A., Acta Met., 8, (1960), 737.

22. Lindley, T.C. and Smallman, R.E., Acta Met., 11, (1963), 626-628.

23. Churchman, A.T., Jour. Inst. Met., 88, (1960), 221-222.

24. Armstrong, W., Bechtold, J.H. and Begly, R.T., AIME and Interscience, New York, 17, (1963), 263.

25. Raghuram, A.C., Reed, R.E. and Armstrong, R.W., J. of Appl. Physics, 40, (1969), 4666-4668.

26. Omar, A.M. and Estwisle, A.R., Mats. Sci. and Eng., 5, (1969-70), 263-270.

27. Tangri, K., Toronchuk, J., and Lloyd, D., Trans. of Ind. Inst. of Met., December 1972.

28. Dunegan, H. and Harris D., Ultrasonics, 7, (1967), 160-166.

29. Schoeck, G., J. of App. Phys., 33, (1962), 1745.

30. Tangri, K. and Tandon, K., Proc.: 4th Bolton Landing Conf., June (1974), 327.

31. Sinha, M.N., Lloyd, D.J., and Tangri, K., J. Mats. Sci. and Eng., 8, (1973), 116-122.

APPENDIX 1

A.1 Introduction

Acoustic emission is the term used to designate the phenomenon of the generation and propagation of acoustic pulses in metals as a result of their deformation.

Sudden stress relaxation in a material gives rise to acoustic pulses, heat and electron emission. Acoustic emission attempts to measure the acoustic pulses. The microscopic processes which occur during the deformation of a material often create some stress relaxation, therefore, acoustic emission from a deforming sample should contain significant information on the processes involved at various stresses and strains. Fairly conclusive evidence shows that most of the acoustic emission observed from metals can be related to pile up and subsequent break away of dislocations as well as from dislocation multiplication, surface effects and crack propagation.

The low energy of acoustic emissions make the use of extremely sensitive and high gain electronic equipment a necessity. For example, pulses of the order of 30×10^{-6} volts are amplified 80 db or more in the present work. Frequencies of acoustic emissions are in the order of 10^5 hz, so that the frequency response of the equipment must be scrutinized carefully before data collection or analysis. The wider the frequency band available the more information one may obtain during experimentation.

The acoustic emission recording and play back block diagrams in Figures 1A and 2A are typical of "state of the art" setups currently in use

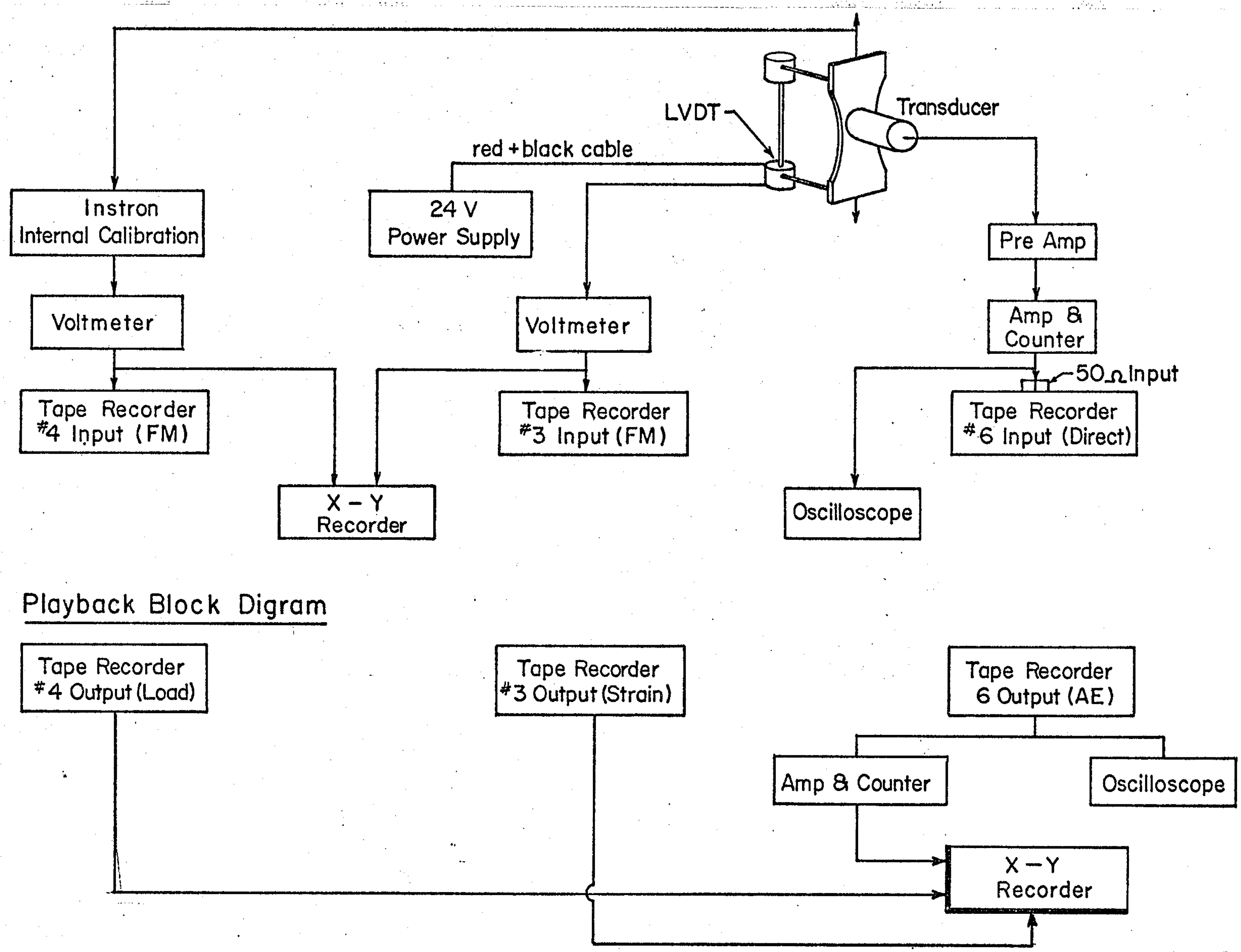

Figure A1: Recording and Playback Block Diagrams.

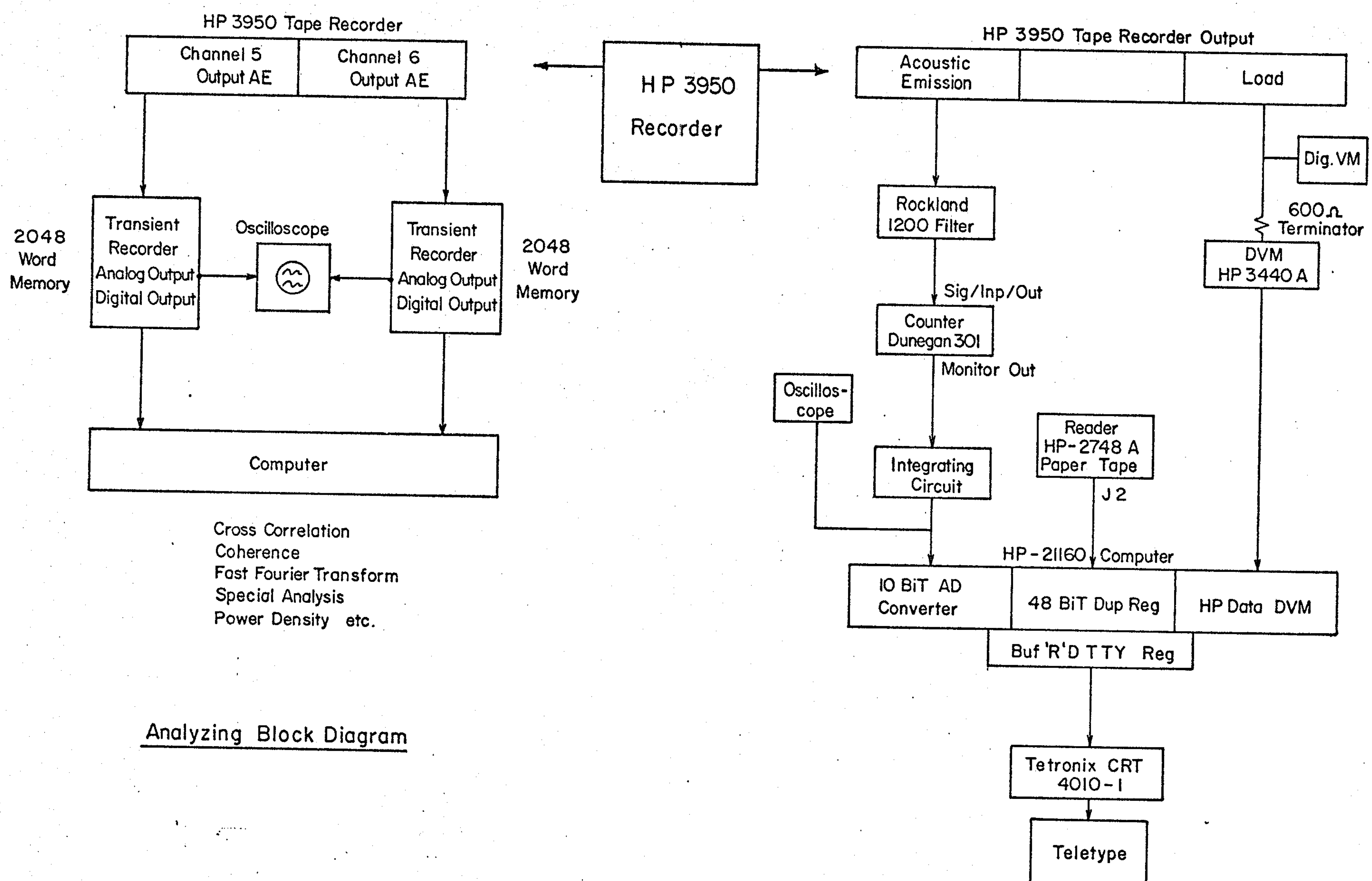

Figure A2: Analyzing Block Diagrams.

for research purposes, and in this laboratory.

Table 1A lists the major components available at the University of Manitoba Materials Science Laboratory for Acoustic Emission Research. Some characteristics of the equipment are listed.

The following section describes, in detail, the procedure undertaken when operating an acoustic emission analysis system such as the one used in the present work.

A.2 Procedure

A.2.1 Instron Calibration

Use two D.V.M.s, one to load cell amp. Set range to 200 mv, other to load data adaptor. Set instron load range selector to minimum range, press zero button and adjust pot to give 0.00 on D.V.M. from load call amp. Release button and use balance controls to rezero meter. Use zero pot on load data adaptor to zero the D.V.M. Add weights and adjust calibrate pot on data adaptor to give correct reading, (1.000 v Full Scale Maximum). Remove weights and check zero. (Load cell amp. maximum 80 mv).

A.2.2 X-Y Recorder

Load data adaptor (LDA) has 1.0 v maximum output, with Y-channel set to 50 mv/cm this gives 20 cm. full scale.

X-channel can be driven with:

(a) ramp generator

(b) LVDT (direct or from tape)

(c) chart motor

(d) strain gauge amplifier (direct or from tape)

A.2.3 Tape Recorder Calibration

Load channel (FM channel 1, 2, 3 or 4) use balance controls to set LDA output to 1.00 volts. Connect to channel input (rear), adjust input gain (front) so that meter on recorder channel reads +1.

LVDT (FM channel) using micrometer move core equivalent to maximum extension required. Connect LVDT output to channel input (rear) and adjust input gain (front) so that channel meter reads +1.

Strain gauge amplifier has full scale setting which can be used to calibrate FM channel as well.

In all cases above channel mode D.C. (front).

A.E. channel (direct) connect function generator to channel input with 600 Ω terminator and also to rms meter and/or scope. Set generator frequency to 400 KHz and output to 1.76 v rms or 5 v peak to peak on scope.

A.E. channel input gain cannot be set until tape is started. Push play, record of tape, allow to settle in, (approximately 50'), then adjust channel input gain to give 0 db on channel meter. Record 400'-500' of calibrate signal.

A.2.4 Tape Recorder Output Calibration

Load channel output cable should have 600 Ω terminator connect to D.V.M., press play, adjust output gain of channel to give 1.00 v. Therefore, input/output 1/1.

Outputs from other DC channels will depend on the voltage input, which determines the input gain. Large voltage inputs (3-10v) require lower input gain and it is not possible to get a one to one input -

output, therefore, the output gain is adjusted to give some convenient fraction of the input. For example, if 10 v input is used, output adjusted to 1 v monitoring devices range changed a factor of 10 on play back. To give same results as original recording.

A.E. channel output calibration one to one input output, therefore, adjust output. Gain to give 5 volts peak to peak on scope of 1.76 volts rms on rms meter.

A.2.5 Experimental Setup

5a Recording

Load signal from LDA to D.V.M. to tape recorder and/or X-Y recorder Y-axis.

L.V.D.T.

24 V D.C. from power supply to input red (+), black (-), coil output to D.V.M. to tape recorder and/or X-Y recorder X-axis.

Strain Gauge Amplifier

Output full scale, 1.41 V or 5 V, or 10 V. To tape recorder and/or X-Y recorder X-axis.

X-Axis Time Base

X-Y recorder chart speeds or ramp generator 0-10 V output.

Acoustic Emission Signal

The transducer picks up the signal from the sample, converts it to an electrical voltage which is transmitted to a fixed gain preamplifier. The amplifier signal is sent to the dunegan 301 totalizer via either

(i) power/signal output/input connection or (ii) signal input/output connection. (Depending on preamplifier used). The signal then passes through the totalizer's variable gain amplifier (0-60 db) to a monitor output connection and a threshold detector. The monitor output connection is used to input the signal to the tape recorder. The threshold detector sends all signals with amplitudes greater than one volt to the counter. The counter converts the number to A.D.C. voltage (0-10 V), which is available at the plotter output. The voltage/number of counts is determined by range selection on front panel.

$$10 \text{ volts} = 10^3\text{c or } 10^4\text{c or } 10^5\text{c or } 10^6\text{c}$$

5b Reproduce

All D.C. signals are outputed directly to which ever monitoring device is being used, either X-Y recorder or computer. The X-Y recorder axis ranges are selected to accommodate what ever the expected full scale voltage will be and give a reasonable chart scale. For example, a 1 V full scale signal will require a 50 mv/cm range selection to give 20 cm full scale. In instances where an L.V.D.T. or strain gauge are used, the outputs may not be unit voltages which will match readily with the recorder ranges, in such a case the nearest range can be selected and the channel amplifier taken out of calibrate and adjusted so that 1 cm will be some even unit of extension or strain. In this situation the channel is only accurate for the particular setting, therefore, switching ranges is not advisable.

When using the computer to analyze data, the load signal must go to the big hp D.V.M. which is part of the computer facility.

A.2.6 Acoustic Emission Signal Play Back

The A.E. signal can be outputed to the X-Y recorder as a D.C. signal (0-10 V) or to the computer.

If X-Y recorder, the signal is taken from tape to rockland filter, to dunegan 301 totalizer via signal input/output jack at rear. The internal amp variable gain should be set to zero unless more gain than recording level is required, and usually not more than 15 → 20 db can be added before tape noise saturates the counter.

The counter converts the A.E. signal to a D.C. voltage (0-10 V) which is available at plotter output (rear) to drive the X-Y recorder Y channel. The counter has ranges $1 = 10^3$, $10 = 10^4$, $100 = 10^5$, $1000 = 10^6$, available as push buttons (front). The signal can be output as totals or rates, with variable time intervals.

To use computer the A.E. signal must be passed through an integrating circuit which converts the signal to a D.C. pulse. The integrator has a baseline attenuation of 12 db which must be compensated for either by informing the computer when entering gain factor, or by adding 12 db in 301 totalizer. The signal flow is: from tape to filter to 301 signal input, through amp. to monitor output, to integrator, to computer.

A.3 To Operate Computer for A.E.

1. Load absolute binary tape into high speed reader.

2. Enter 017700* in switch register, loader switch to enabled, press load address, preset, and run. Allow punched tape to be read into computer, loader switch to protected.
3. The following instructions must be entered at the correct address through the switch register:
   (i) 10, load address, 115000, load memory
   (ii) 12, load address, 115001, load memory
   (iii) 1000, load address, 002340, load memory
   (iv) 1001, load address, 002201, load memory
   (v) 2000, load address, preset, run.
4. The computer responds with a series of teletype messages, each requiring an answer about a particular variable before proceeding. The messages are in the form Ent 1 → Ent 5 start, the operator must make an entry then punch return, line feed.

Ent 1

Variable: Enter gain factor in db return (RT), line feed (LF).

Ent 2

Variable: Total test time in (- seconds) RT, LF.

Ent 3

Variable: Load cell scale in Kg. RT, LF.

---

*Switch register on octal numbers. See following section (A.4).

Ent 3A

Variable: Load cell voltage offset (MV) RT, LF.

Ent 4

Variable: Voltmeter scale in volts RT, LF. (Usually 1).

Ent 5

Variable: Spare, not used (enter 1). RT, LF.

Start

Enter 0, return, line feed. The line feed should be given when the mag. tape reaches the desired starting footage mark. Computer will sample inputs at one second intervals for test duration as indicated in Ent 2. At the end of this time, sampling will stop, and the computer will give the message Ent 7. The mag. tape must be stopped.

Ent 7

Variable: 3 option 0 - restart

1 - hard copy

3 - graphics

If 0 enter 0, RT, LF. Go to computer press halt, preset, run, and computer will give Ent 1 to start again.

If 1 enter 1, RT, LF and computer operate teletype to print out results, i.e., Load, Rate, Totals, Au. amp., Peak amp., v^2t, Aum v^2.

If 3 enter 3, RT, LF. Computer will give Ent 8.

Ent 8

Variable: Division of graphics outline 1, 2, or 3 usually 2 RT, LF, computer gives Ent 9.

Ent 9

Variable: 7 options 0 - load

2 - rate

4 - totals

6 - AV amplitude (μv)

8 - peak amplitude (μv)

10 - v^2t (total energy of sample)

12 - AV v^2 (average energy/event)

RT. LF, computer gives Ent 10.

Ent 10

Variable: Dimension of variable chosen in Ent 9, with decimal point.

Example:

Ent 9 = 0 RT, LF Ent 10 = 500.0 RT, LF.

Computer will graph out results and give Ent 7 again. This Ent 7 will not be visable, as it will be buried in some nonsense at the lower left corner of the CRT, and when switching back to the teletype for further instructions a cue is lost and it is necessary to enter, RT, LF. The next command twice.

Example:

Ent 10 → Enter proper dimension, RT, LF, immediately switch graphics terminal to local, variable is plotted, switch back to line, and teletype is in control. To graph another variable, enter 3, RT, LF, nothing happens, enter 3, RT, LF and computer gives Ent 8, and the process starts over.

5. Variables can be plotted on top of each other or the CRT can be cleared by pressing "page" on the graphics terminal.

A.4 HP 2116-C Computer Switch Register

The switch register has sixteen (16) off/on toggle switches (0, 1, 2, 3 . . . 15), and a series of function push buttons (example, run, halt, load address, load memory, etc.).

The off/on of the toggle switches corresponds to the binary number system 0, 1.

A sixteen digit binary number is awkward to work with, but a group of three binary numbers constitutes an octal number. This reduces the register to a more workable six digits.

Examples:

15	14 13 12	11 10 9	8 7 6	5 4 3	2 1 0
0	1 0 1	1 0 0	0 1 1	0 1 0	0 0 1
0 OCTAL	5 OCTAL	4 OCTAL	3 OCTAL	2 OCTAL	1 OCTAL
1	0 0 0	0 0 0	0 0 0	1 1 1	1 1 0
1 OCTAL	0 OCTAL	0 OCTAL	0 OCTAL	7 OCTAL	6 OCTAL

BINARY	OCTAL
0/101/100/011/010/001	054321
1/000/000/000/111/110	100076

TABLE 1A

LIST OF COMPONENTS

(a) Transducers

Narrow Band

S140A	Dunegan	140-160 KHz (-80 → -90 db)
S141B	Dunegan	40-95 KHz (-80 → -93 db)
S450B	Dunegan	375-475 KHz (-80 → -85 db)
S1MB	Dunegan	.7 → 1.4 MHz (-76 → -87 db)
S140B/LD	Dunegan	100 → 180 KHz
S9220	Dunegan	150 KHz (Very sharp) Micro Miniture 1000°F
S9205M2	Dunegan	100 → 200 KHz
AC750	Acoustic Emission Technical Corp.	200 → 800 KHz (-80 → 100 db)
AC175L	Acoustic Emission Technical Corp.	180 → 220 KHz (-80 → -90 db)

Wide Band

S9201	Endevco	.1 → 1.0 MHz (-76 db)
FC500	A.E.T.C.	.2 → 1.5 MHz (Flat -92 db) ±2 db

(b) Preamplifiers

2 Dunegan Research Corporation Model 801P 40 db gain

(c) Signal Conditioners and Accessories

Dunegan Corp. Model 301 Totalizer

- Variable gain 0 → 60 db

Dunegan Corp. Model 302 Signal Conditioner

- Variable gain 0 → 60 db

Dunegan Corp. Model 402 Reset Clock

- Variable .1 sec to 20 min

Dunegan Corp. Model 905 Digital Envelope Processor

- Variable .01 → 10 mins

Dunegan Corp. Model 502 Ramp Generator

(d) Recorders

Hewlett Packard Model 3950 Magnetic Tape Recorder

- 7 channel 4FM + 3 Direct
- Speeds 3 3/4, 7 1/2, 15, 30, 60, 120 in/sec ± .03%
- Freq. Resp. .4-750 KHz with S/N ratio 29 db @ 60 in/s

Biomation Model 805 Transient Recorder

- input Band width DC to 1.25 MHz
- Memory 8 bits x 2048 words
- Sample Interval .2 m sec to 100 m sec
- record time

  1048 x sample interval, variable between .4 ms to 200 s

(e) Filter

Rockland Model 1200

- Variable between 0 and 1 MHz
- Bandpass and band reject
- Bessel and Butterworth functions

(f) Computer and Hardware

Hewlett-Packard Model 2118C. Computer

- Memory 8K

Hewlett-Packard Model 3440A. Digital Voltmeter

Hewlett-Packard Model 2748A. Tape Reader

Teletype

C.R.T.

(g) Accessories

Oscilloscope - Dual Beam Model 7613

Hewlett-Packard Model 331A Function Generation

Hewlett-Packard Model 77404B X-Y Recorder

Hewlett-Packard Model 400E AC Voltmeter

Hewlett-Packard Model 3403C True RMS Voltmeter

Hewlett-Packard Model 6289A DC Power Supply

Accudata Model 218 Bridge Amplifier

Fluke Model 8000A Digital Multimeter

Keithley Model 160 Digital Multimeter